The EMBO Journal (2010) 29, 2899–2914 | © 2010 European Molecular Biology Organization | All Rights Reserved 0261-4189/10
www.embojournal.org

THE EMBO JOURNAL

Calmodulin dissociation regulates Myo5 recruitment and function at endocytic sites

Helga Grötsch[1,2], Jonathan P Giblin[1], Fatima-Zahra Idrissi[1,6], Isabel-María Fernández-Golbano[1,6], John R Collette[3,4], Thomas M Newpher[3,5], Virginia Robles[1], Sandra K Lemmon[3] and María-Isabel Geli[1,*]

[1]Department of Cellular Biology, Instituto de Biología Molecular de Barcelona (IBMB-CSIC), Barcelona, Spain, [2]Department of Paediatrics and Adolescent Medicine, University-Hospital Schleswig-Holstein, University of Lübeck, Lübeck, Germany, [3]Department of Molecular and Cellular Pharmacology, University of Miami, Miami, FL, USA, [4]Department of Microbiology and Molecular Genetics, University of Texas at Houston Medical School, Houston, TX, USA and [5]Department of Neurobiology, Duke University Medical Center, Durham, NC, USA

Myosins-I are conserved proteins that bear an N-terminal motor head followed by a Tail Homology 1 (TH1) lipid-binding domain. Some myosins-I have an additional C-terminal extension (C_{ext}) that promotes Arp2/3 complex-dependent actin polymerization. The head and the tail are separated by a neck that binds calmodulin or calmodulin-related light chains. Myosins-I are known to participate in actin-dependent membrane remodelling. However, the molecular mechanisms controlling their recruitment and their biochemical activities *in vivo* are far from being understood. In this study, we provided evidence suggesting the existence of an inhibitory interaction between the TH1 domain of the yeast myosin-I Myo5 and its C_{ext}. The TH1 domain prevented binding of the Myo5 C_{ext} to the yeast WIP homologue Vrp1, Myo5 C_{ext}-induced actin polymerization and recruitment of the Myo5 C_{ext} to endocytic sites. Our data also indicated that calmodulin dissociation from Myo5 weakened the interaction between the neck and TH1 domains and the C_{ext}. Concomitantly, calmodulin dissociation triggered Myo5 binding to Vrp1, extended the myosin-I lifespan at endocytic sites and activated Myo5-induced actin polymerization.

The EMBO Journal (2010) **29,** 2899–2914. doi:10.1038/emboj.2010.159; Published online 20 July 2010
Subject Categories: membranes & transport; cell & tissue architecture
Keywords: Arp2/3 complex; calmodulin; endocytosis; myosin-I; WIP-Vrp1

*Corresponding author. Department of Cellular Biology, Instituto de Biologia Molecular de Barcelona (IBMB-CSIC), Baldiri Reixac 15, Barcelona 08028, Spain. Tel.: +34 93 402 0193; Fax: +34 93 403 4979; E-mail: mgfbmc@ibmb.csic.es
[6]These authors contributed equally to this work

Received: 31 July 2009; accepted: 21 June 2010; published online: 20 July 2010

Introduction

Myosins-I are widely expressed actin-dependent molecular motors, which share a conserved structural organization. Besides the N-terminal actin-activated ATPase that translocates actin filaments, all myosins-I bear a Tail Homology 1 (TH1) domain that binds acidic phospholipids *in vitro* (Pollard *et al*, 1991). The motor head and the TH1 domain are separated by an α helical neck that associates with calmodulin or calmodulin-related light chains (Pollard *et al*, 1991). In addition, the so-called long-tailed myosins-I bear a C-terminal extension (C_{ext}), which can trigger Arp2/3 complex-dependent actin polymerization. The C_{ext} includes a Tail Homology 2 (TH2) domain, which binds filamentous actin (Pollard *et al*, 1991) and a Src Homology 3 (SH3) domain, which associates with proline-rich motifs (Kuriyan and Cowburn, 1997). The fungal myosins-I also bear an acidic peptide, which directly participates in the activation of the Arp2/3 complex (Evangelista *et al*, 2000; Lechler *et al*, 2000, 2001; Lee *et al*, 2000; Idrissi *et al*, 2002; Sun *et al*, 2006) (Figure 1B). The protozoal and the long-tailed mammalian myosins-I lack this acidic peptide but might indirectly activate the Arp2/3 complex through association with CARMIL (Jung *et al*, 2001).

Myosins-I participate in a number of processes requiring actin-dependent remodelling or movement of cellular membranes. These include clathrin-dependent endocytic budding in yeast and mammals (Geli and Riezman, 1996; Sun *et al*, 2006; Krendel *et al*, 2007), vacuole contraction, cell motility, phagocytosis and pinocytosis in protozoa (Jung and Hammer, 1990; Wessels *et al*, 1991; Doberstein *et al*, 1993; Titus *et al*, 1993; Novak *et al*, 1995; Novak and Titus, 1997), and membrane traffic along the endocytic and secretory pathways in protozoa and higher eukaryotes (Fath *et al*, 1994; Durrbach *et al*, 1996, 2000; Temesvari *et al*, 1996; Raposo *et al*, 1999; Huber *et al*, 2000; Neuhaus and Soldati, 2000; Cordonnier *et al*, 2001; Bose *et al*, 2002). Thus, myosin-I function requires its precise targeting and/or activation at particular membrane subdomains. Despite intense research on these proteins, the mechanisms that spatially and temporally define their recruitment and/or regulate their biochemical activities *in vivo* are poorly understood.

The yeast long-tailed myosin-I Myo5, and its homologue Myo3, are well-characterized members of the myosin-I family. Myo5 and Myo3 participate in the formation of endocytic vesicles at the plasma membrane (PM) (Geli and Riezman, 1996). Myo5 is recruited to endocytic sites labelled with clathrin, stays anchored at the PM for 10 to 15 s and disappears around the time the endocytic coat moves into the cytosol (Jonsdottir and Li, 2004; Sun *et al*, 2006). During the transient association of the myosins-I with the endocytic sites, their mechanochemical activity and their actin polymerization promoting activity contribute to vesicle budding (Sun *et al*, 2006; Galletta *et al*, 2008; Idrissi *et al*, 2008).

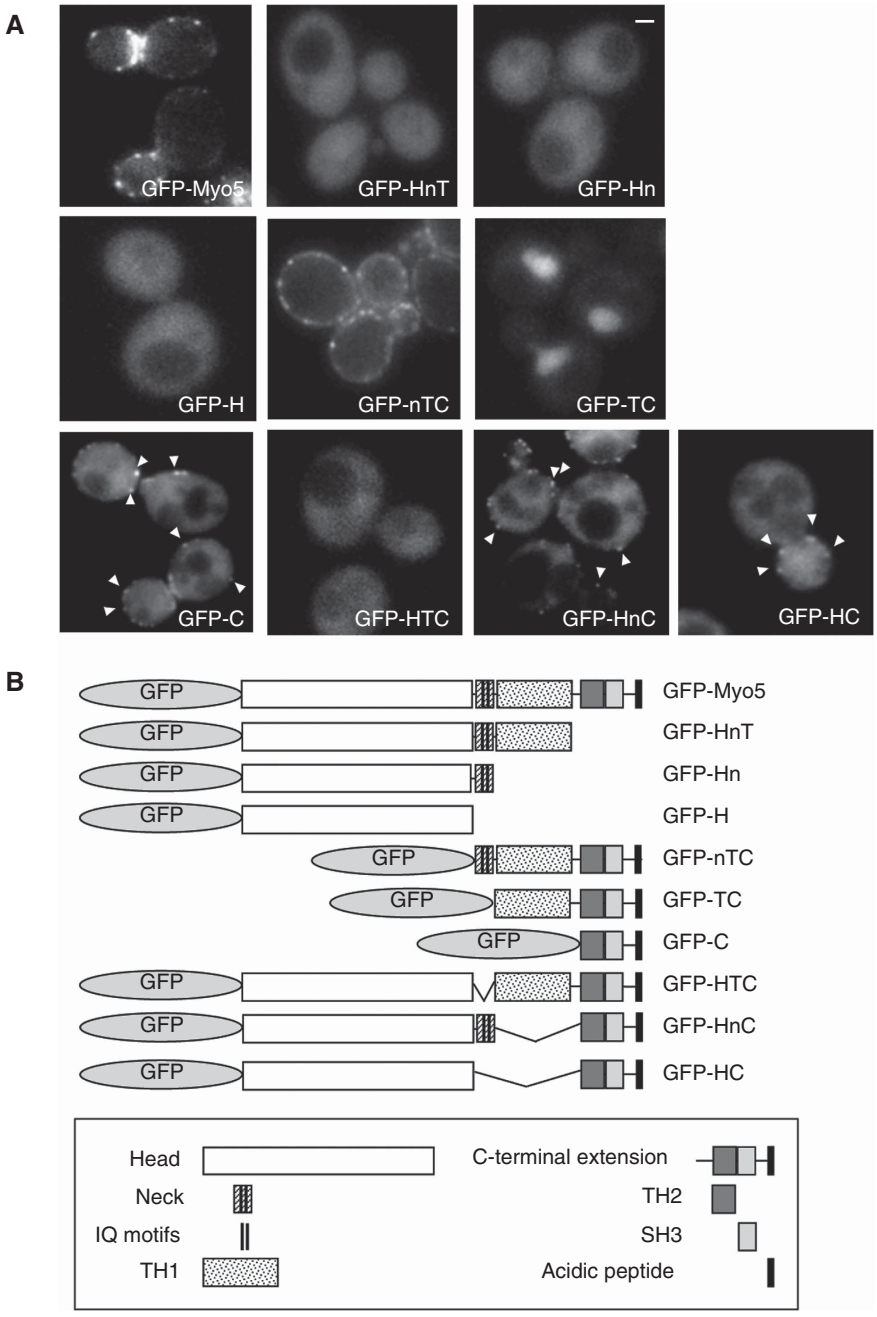

Figure 1 Subcellular localization of GFP-Myo5 constructs. (**A**) Fluorescence micrographs of live *myo5*Δ cells (SCMIG275), expressing the indicated GFP fusion proteins represented in (**B**) expressed from centromeric plasmids under the control of the *MYO5* promoter. Cells were grown to mid-log phase at 25°C and observed by conventional fluorescence microscopy. Arrowheads indicate cortical patches. Bar = 1 μm.

Myo5 recruitment at cortical patches is at least partially dependent on its SH3 domain. Mutation of this domain or deletion of the SH3 interacting partners Vrp1/WIP (WASP-interacting protein) or Las17/WASP (Wiskott–Aldrich syndrome protein) causes partial mislocalization of the myosin to the cytosol (Anderson *et al*, 1998; Sun *et al*, 2006). Intriguingly, Vrp1 and Las17 arrive significantly earlier than the myosin at the endocytic sites, indicating that their association with Myo5 might be regulated (Jonsdottir and Li, 2004; Sun *et al*, 2006). On the other hand, domains other than the SH3 are involved in the cortical recruitment of Myo5 as the SH3 domain alone does not localize to endocytic patches (Anderson *et al*, 1998).

In this study, we provided evidence indicating the existence of an inhibitory interaction between the TH1 domain and the C_{ext}, which prevented Myo5 binding to Vrp1. Interestingly, we found that dissociation of Cmd1 from the Myo5 neck weakened the interaction between a fragment containing the neck and TH1 domain and the C_{ext}. Concomitantly, Cmd1 dissociation promoted binding of Myo5 to Vrp1. Consistent with previous observations indicating that Vrp1 participates in Myo5 recruitment to cortical endocytic sites (Anderson *et al*, 1998; Sun *et al*, 2006) and that Vrp1 is required to trigger Myo5-induced actin polymerization (Geli *et al*, 2000; Lechler *et al*, 2001; Sun *et al*, 2006), we found that Cmd1 dissociation from the myosin elongated

its lifespan at cortical endocytic sites and triggered Myo5-induced actin polymerization *in vivo* and *in vitro*.

Results

The Myo5 TH1 domain interacts with the C_{ext} and negatively regulates association with Vrp1 and recruitment to endocytic sites

To analyse the function of different domains in the recruitment of Myo5 to cortical patches, we investigated the localization of GFP-tagged full-length or truncated Myo5 by fluorescence microscopy (Figure 1). As previously shown, full-length Myo5 (GFP-Myo5) concentrated at cortical patches that partially colocalized with endocytic markers (Figure 1A; Supplementary Figure S1A) (Anderson *et al*, 1998; Jonsdottir and Li, 2004; Sun *et al*, 2006). In addition, a diffuse PM and a weak cytosolic staining were observed. Consistent with the observation that the SH3 domain is required for Myo5 localization (Anderson *et al*, 1998), truncation of the C_{ext} (GFP-HnT) impaired cortical patch recruitment (Figure 1A). On the other hand, we found that the complete C_{ext} (GFP-C) was recruited to endocytic sites (Figure 1A; Supplementary Figure S1A), even though a strong cytosolic signal was also observed for this construct. The overexpression of GFP-C compared with GFP-Myo5 could account for the partial mislocalization of the C_{ext} (Supplementary Figure S1B). In addition, the absence of the TH1 lipid-binding domain, which targets other myosins-I to specific cellular membranes, could partially impair proper recruitment of Myo5 to the PM. However, we observed that addition of amino acids 774 to 996 of the TH1 domain to the C_{ext} (GFP-TC) did not improve Myo5 localization but rather mistargeted the myosin to the cytosol and the nucleus (Figure 1A). Interestingly, cortical patch localization was recovered with addition of the neck and 15 amino acids of the N-terminus of the TH1 domain (GFP-nTC) (Figure 1A; Supplementary Figure S1A). These results suggested that the Myo5 neck might be required to release an inhibitory interaction between the TH1 domain and the C_{ext}. Consistent with this hypothesis, a GFP fusion protein lacking only the neck (GFP-HTC) lost the cortical patch localization, which was partially recovered by deletion of the TH1 (GFP-HC) (Figure 1A; Supplementary Figure S1A). Conversely, a GFP fusion protein missing only the TH1 domain (GFP-HnC) was still recruited to endocytic sites (Figure 1A; Supplementary Figure S1A), although the absence of the TH1 domain again increased the cytosolic signal.

Binding of the Myo5 C_{ext} to Vrp1 participates in the myosin recruitment to endocytic patches (Anderson *et al*, 1998; Sun *et al*, 2006). Therefore, we next investigated whether the presence of the TH1 domain interfered with Myo5 binding to Vrp1 in the absence of the neck. Extracts of yeast cells expressing different Protein A (PA)-tagged Myo5 constructs and haemagglutinin (HA)-tagged Vrp1 (Vrp1-HA) were subjected to IgG pull downs. The presence of Vrp1-HA in the precipitates was detected by immunoblotting. As shown in Figures 1A and 2A, a correlation between the cortical patch localization and Vrp1-HA binding was observed for the different constructs. Thus, a construct bearing the Myo5 C_{ext} (PA-C) pulled down Vrp1-HA but addition of a TH1 domain (PA-TC) blocked the interaction. Further, the presence of the Myo5 neck and 15 amino acids of the N-terminus of the TH1 domain (PA-nTC) recovered Vrp1-HA binding to levels similar to the wild-type (wt) myosin. Also consistent with our model, deletion of the TH1 domain (PA-HnC) significantly increased binding of Myo5 to Vrp1-HA, whereas deletion of the neck (PA-HTC) completely abolished the interaction. Deletion of the neck did not seem to grossly affect the structure of the tail as the PA-HTC construct still bound to Rvs167 similar to the wt protein (Geli *et al*, 2000; Tong *et al*, 2002) (Figure 2B).

Previous results suggested an intramolecular interaction between the TH1 domain and the C_{ext} of the protozoal long-tailed myosins-I (Jontes *et al*, 1998; Lee *et al*, 1999; Ishikawa *et al*, 2004; Hwang *et al*, 2007). We failed to express significant amounts of the TH1 domain alone, but pull-down experiments using the C_{ext} fused to GST (GST-C) and yeast extracts expressing PA-tagged Myo5 truncations bearing the H, Hn, HT and HnT fragments demonstrated a specific interaction between the C_{ext} and the TH1 domain, which seemed to be stabilized by the presence of the neck (Figure 2C). The interaction between the nT fragment and the C_{ext} was direct, as the nT fragment could be overlaid with GST-C purified from *Escherichia coli* (Figure 2D).

To analyse whether the nT fragment interfered with the C_{ext}-dependent Myo5/Vrp1 interaction, PA-C was pulled down from yeast expressing Vrp1-HA and overexpressing LexA fused to the Myo5 neck and TH1 domains (LexA-nT) or LexA fused to Rvs167 as a control. As shown in Figure 2E, LexA-nT was pulled down with the C_{ext} and significantly interfered with the Myo5/Vrp1 interaction when compared with LexA-Rvs167. The Vrp1-HA signal was reduced 6.57 ± 1.02-fold ($n = 3$) in the pull downs from cells expressing LexA-nT with respect to those expressing LexA-Rvs167. The inhibitory domain was contained within the TH1 domain as a LexA-n construct still interacted with PA-C but failed to interfere with Vrp1-HA binding (Figure 2E).

Cmd1 dissociation from the Myo5 neck weakens the neck-TH1/C_{ext} interaction and promotes Myo5 binding to Vrp1

Our results suggested that the neck and the TH1 domains interact with the Myo5 C_{ext}, that the TH1 domain interferes with Myo5 binding to Vrp1 and that the adjacent Myo5 neck modulates the release of the neck-TH1/C_{ext} interaction. To investigate whether calmodulin association/dissociation from the Myo5 neck might influence Myo5 binding to Vrp1, PA-Myo5 was precipitated with IgG-Sepharose from an extract of yeast expressing Vrp1-HA in the absence or presence of 5 mM $CaCl_2$. The Myo5 neck contains two IQ motifs, which bind calmodulin in the absence of Ca^{2+}. Addition of 5 mM $CaCl_2$ triggers dissociation of calmodulin (Geli *et al*, 1998). As shown in Figure 3A, addition of calcium significantly reduced Cmd1 association to Myo5 and concomitantly increased the Myo5/Vrp1 interaction. Vrp1 specifically bound PA-Myo5 as deletion of the C_{ext} (PA-HnT) completely eliminated the Vrp1-HA signal (Figure 3A). To demonstrate that Cmd1 dissociation and not the $CaCl_2$ treatment *per se* increased Vrp1 binding, we used myosin and calmodulin mutations that specifically disrupt the Cmd1/Myo5 interaction in the absence of calcium: *myo5-iq*Δ and *cmd1-226* (Geli *et al*, 1998). The IQ motifs required for Cmd1 binding (IQRAWRRFLQR and IQRTIRERKEG) are deleted in the Myo5-iqΔ mutant. The mutant loses its capacity to interact with Cmd1 but, in contrast to the HTC construct, it retains a portion of the

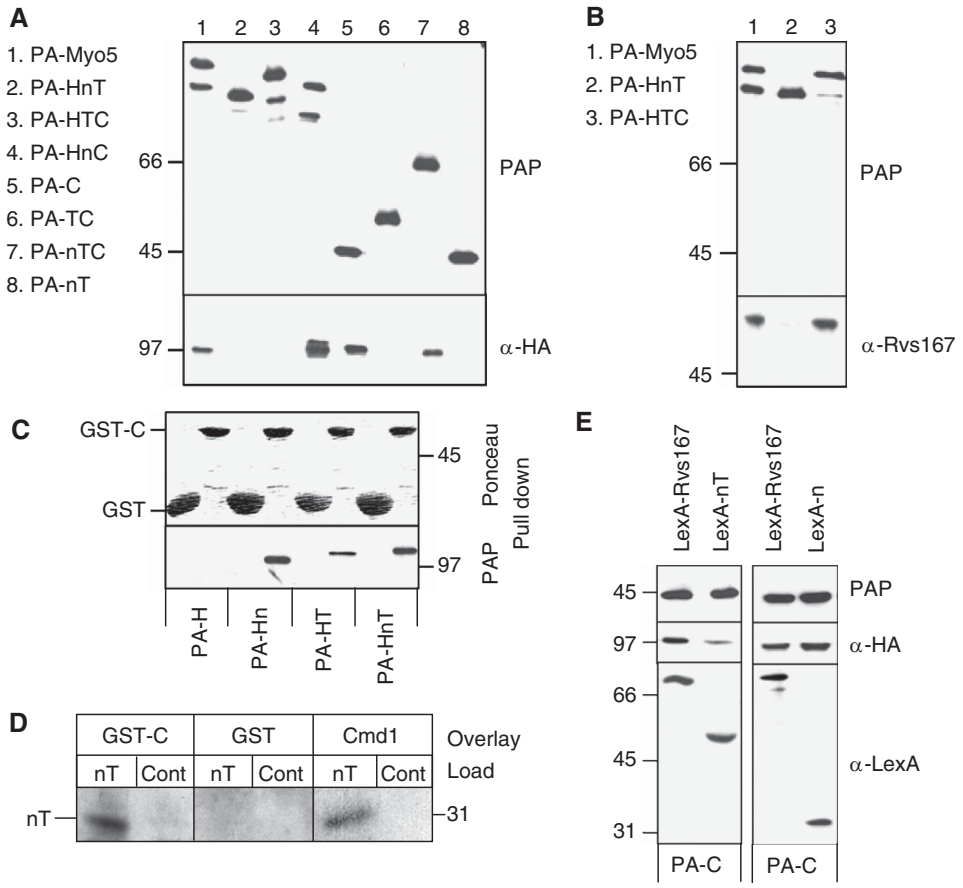

Figure 2 The Myo5 TH1 domain blocks the interaction of the Myo5 C_{ext} with Vrp1. (**A**, **B**, **E**) Immunoblots of IgG-Sepharose pull downs from *myo5*Δ *vrp1*Δ cells (SCMIG304), expressing the indicated PA-Myo5 constructs and Vrp1-HA, either overexpressing (**E**) or not (**A**, **B**) the indicated LexA fusion proteins (**E**). PAP, a peroxidase-conjugated anti-HA antibody and anti-Rvs167 or anti-Cmd1 antibodies, combined with the adequate peroxidase-conjugated secondary antibody, were used for detection of the PA-Myo5 constructs, Vrp1-HA, Rvs167 and Cmd1, respectively. All PA-Myo5 constructs and Vrp1-HA were expressed from centromeric plasmids under the control of their own promoters. (**C**) Immunoblot of glutathione-Sepharose pull downs of GST-C or GST, incubated with extracts of a *myo5*Δ strain (SCMIG275), expressing the indicated PA-Myo5 constructs from centromeric plasmids under the *MYO5* promoter, decorated with Ponceau red to detect GST-C and GST or PAP to detect the PA-Myo5 constructs. (**D**) Overlay assay of an Myo5 nT fragment, partially renatured after SDS–PAGE and western blot, incubated with 20 mM GST or GST fused to the Myo5 C_{ext} (GST-C) or 60 mM Cmd1. GST and Cmd1 were detected using anti-GST and anti-Cmd1 antibodies and the adequate peroxidase-conjugated secondary antibodies. Control lanes (Cont) were loaded with residual proteins that might elute from the IgG-Sepharose under the conditions used for the nT purification, derived from a strain not expressing the PA-nT fragment.

neck. The Cmd1-226 mutant bears an F92A substitution, which specifically disrupts the Cmd1/Myo5 interaction (Ohya and Botstein, 1994; Geli *et al*, 1998). Consistent with our hypothesis, the *cmd1-226* mutation significantly decreased association of PA-Myo5 with Cmd1 and concomitantly increased binding to Vrp1, as compared with the wt *CMD1* or with the *cmd1-231* mutation, which does not affect the Myo5/Cmd1 interaction (Figure 3B) (Geli *et al*, 1998). The Myo5-iqΔ mutant did not bind Cmd1 and it coprecipitated significant amounts of Vrp1 in the absence or presence of calcium (Figure 3A). However, Myo5-iqΔ bound slightly less Vrp1-HA than the intact calmodulin-stripped Myo5. The Vrp1-HA signal appeared 3 ± 0.7-fold increased in the Myo5-iqΔ pull downs compared with the Cmd1-bound Myo5 ($n = 3$), whereas calmodulin stripping from the wt Myo5 resulted in a 9 ± 3.4-fold increase of the Vrp1-HA signal ($n = 3$). The result suggested that an intact neck might be required to completely release the nT/C interaction. Deletion of individual IQ motifs did not seem to have a major influence in Myo5 binding to Vrp1, suggesting that full activation required dissociation of Cmd1 from both IQ motifs (Supplementary Figure S2A).

To investigate whether association of Cmd1 to the myosin neck could influence the affinity of the nT fragment and the C_{ext}, purified PA-nT was incubated with GST fused to the C_{ext} (GST-C), in the presence or absence of 5 mM $CaCl_2$ (Figure 3C). In the presence of 5 mM $CaCl_2$ Cmd1 dissociated from the nT fragment (Figure 3C) (Geli *et al*, 1998). Concomitantly, the presence of $CaCl_2$ triggered dissociation of PA-nT from the C_{ext} (Figure 3C). Dissociation of Cmd1 also disrupted the interaction between the PA-Hn and PA-HnT fragments and the C_{ext} but did not have an influence on the PA-HT/C or the PA-HnT-iqΔ/C interactions (Supplementary Figure S3A).

To demonstrate that association of Cmd1 to the myosin neck could reversibly influence the affinity between the Myo5 fragments, Cmd1-free PA-nT was incubated with GST-C-coated beads, in the presence or absence of recombinant purified Cmd1. As shown in Figure 3D, Cmd1 binding favoured the interaction of PA-nT with the C_{ext}.

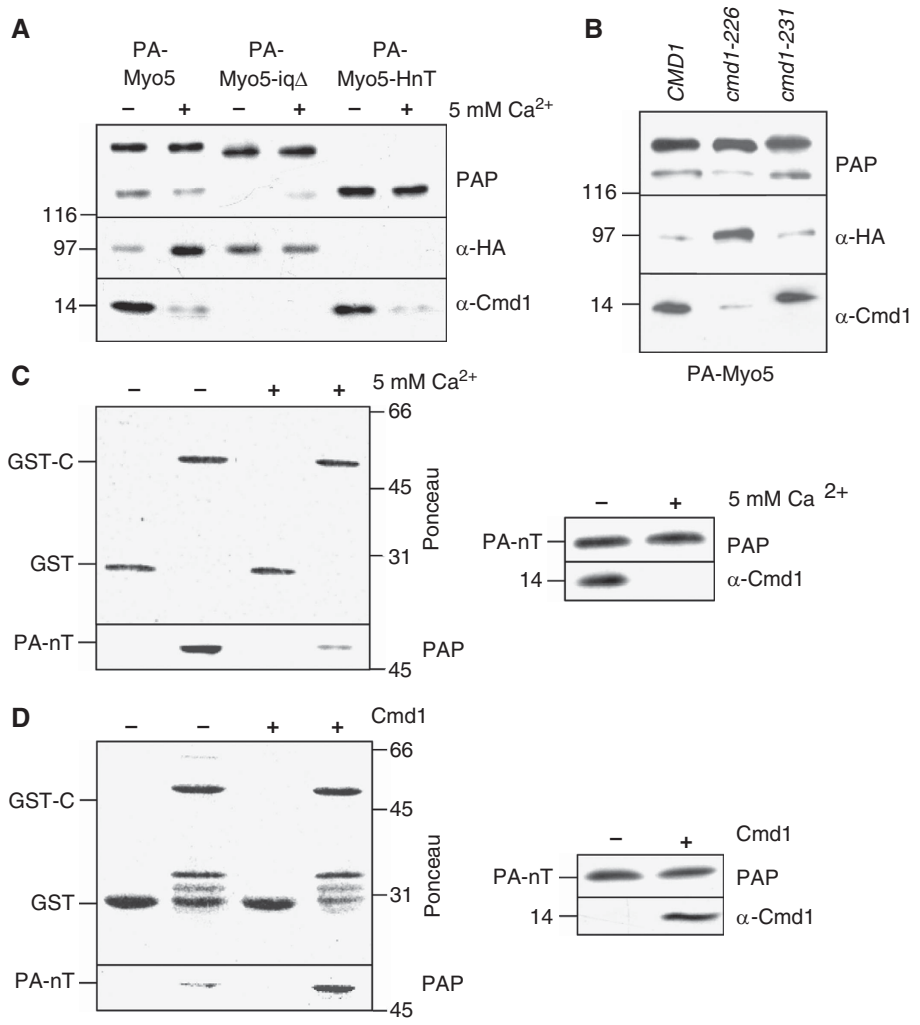

Figure 3 Cmd1 dissociation promotes Myo5 binding to Vrp1 and weakens the nT/C interaction. (**A**, **B**) Immunoblots of IgG-Sepharose pull downs from *myo5*Δ *vrp1*Δ cells (SCMIG304) (**A**) or wt (*CMD1*, SCMIG947), *cmd1-226* (SCMIG182) and *cmd1-231* (SCMIG187) strains (**B**), expressing the indicated PA-Myo5 constructs and Vrp1-HA in the absence (**A**(−), **B**) or in the presence 5 mM $CaCl_2$ (**A** (+)) to trigger Cmd1 dissociation. PAP, a peroxidase-conjugated anti-HA antibody and an anti-Cmd1 antibody combined with the adequate peroxidase-conjugated secondary antibody were used for detection of the PA-Myo5 constructs, Vrp1-HA and Cmd1, respectively. All PA-Myo5 constructs and Vrp1-HA were expressed from centromeric plasmids under the control of their own promoters. (**C**) Immunoblot of glutathione-Sepharose pull downs of GST-C or GST, incubated with PA-nT, purified in the absence (−) or presence (+) of 5 mM $CaCl_2$ to trigger Cmd1 dissociation. Ponceau, PAP and an anti-Cmd1 antibody, combined with the appropriate secondary antibody, were used for detection of GST-C and GST, PA-nT and Cmd1, respectively. (**D**) Immunoblot of GST-C or GST incubated with Cmd1-free PA-nT, in the absence (−) or presence (+) of 50 nM of recombinant purified Cmd1, processed as in (**C**).

Cmd1 dissociation from Myo5 extends the myosin lifespan at cortical patches

As Vrp1 participates in the recruitment of Myo5 to cortical endocytic patches *in vivo*, we next investigated whether Cmd1 also controlled Myo5 association to endocytic sites using live-cell imaging. Under the experimental conditions used, no significant endocytic defects are observed in the *myo5-iq*Δ and *cmd1-226* mutants (Geli *et al*, 1998) and consistently, no significant difference in the dynamics of the clathrin-coat component Sla1-mCherry at cortical patches could be observed for the different mutants, as compared with the isogenic wts (Table I, SCMIG1079 p*GFP-MYO5* versus SCMIG1079 pGFP-*myo5-iq*Δ and SCMIG1077 p*GFP-MYO5* versus SCMIG1078 p*GFP-MYO5*, mCherry channel). In contrast, the lifespan of GFP-Myo5 significantly increased in mutants that disrupted the Myo5/Cmd1 interaction (*GFP-myo5-iq*Δ and *cmd1-226*, Table I, GFP channel and Figure 4A and B). The average lifespan of GFP-Myo5 in different strain backgrounds expressing the wt Cmd1 was 12 to 13.1 s, whereas it was extended up to 19.5 s in strains where the Myo5/Cmd1 interaction was disrupted (Table I, GFP channel and Figure 4A and B). A fraction of the GFP-Myo5 cortical patches still exhibited wt dynamics under conditions that disrupted the Myo5/Cmd1 interaction. However, about 50% of the patches had lifespans longer than 16 s in the *cmd1-226* mutant (versus only <8% in the isogenic wts) (Figure 4C and D). Consistent with the observation that an intact neck was required to fully promote binding of Myo5 to Vrp1, the Myo5-iqΔ mutant was slightly less efficient than the *cmd1-226* mutant in extending the Myo5 lifespan at cortical sites (Table I, the lifespan of Myo5-iqΔ was 14.7 s, versus >15.9 s for the wt Myo5 in the *cmd1-226* mutants). The extension of the Myo5 lifespan at cortical sites was specific for the conditions that disrupted the Myo5/Cmd1 interaction as deletion of

Table I Lifespans of GFP-Myo5, Sla1-mCherry and Abp1-RFP patches in mutants that disrupt the Myo5/Cmd1 interaction

Channel	RFP/mCherry				GFP			
Strain	Avg	s.d.	*n*	*P*	Avg	s.d.	*n*	*P*
GFP-MYO5 (Y06549 p*GFP-MYO5*)	—	—	—		12.1	3.5	80	
*GFP-myo5-iq1*Δ (Y06549 p*GFP-myo5-iq1*Δ)					13.7	3.4	80	0.003
*GFP-myo5-iq2*Δ (Y06549 p*GFP-myo5-iq2*Δ)					12.8	3.3	80	0.1
*GFP-myo5-iq*Δ (Y06549 p*GFP-myo5-iq*Δ)	—	—	—	—	14.7	5.2	80	1×10^{-4}
CMD1 GFP-MYO5 (SCMIG1057 p*GFP-MYO5*)	—	—	—		12.2	3.7	80	
cmd1-226 GFP-MYO5 (SCMIG1058 p*GFP-MYO5*)	—	—	—	—	15.9	4.9	80	1×10^{-4}
cmd1-231 GFP-MYO5 (SCMIG1059 p*GFP-MYO5*)	—	—	—	—	13.2	4.6	80	0.2
GFP-MYO5 SLA1-mCherry (SCMIG1079 p*GFP-MYO5*)	23.3	4.9	57		ND	ND	ND	
*GFP-myo5-iq*Δ *SLA1-mCherry* (SCMIG1079 p*GFP-myo5-iq*Δ)	21.7	3.9	57	0.3147	ND	ND	ND	ND
CMD1 GFP-MYO5 SLA1-mCherry (SCMIG1077 p*GFP-MYO5*)	24.6	4.4	51		13.1	3.3	51	
cmd1-226 GFP-MYO5 SLA1-mCherry (SCMIG1078 p*GFP-MYO5*)	24.12	4.4	51	0.5310	18.4	6.5	51	2×10^{-6}
GFP-MYO5 ABP1-RFP (SCMIG880 p*GFP-MYO5*)	14.1	3.2	52		ND	ND	ND	
*GFP-myo5-iq*Δ *ABP1-RFP* (SCMIG880 p*GFP-myo5-iq*Δ)	21.6	7.3	54	7×10^{-10}	ND	ND	ND	ND
CMD1 GFP-MYO5 ABP1-RFP (SCMIG1063 p*GFP-MYO5*)	13.4	4.5	56		12.3	4.5	59	
cmd1-226 GFP-MYO5 ABP1-RFP (SCMIG1064 p*GFP-MYO5*)	18.5	5.7	58	8×10^{-7}	19.5	5.7	52	8×10^{-11}

The average (avg) and standard deviation (s.d.) are indicated in seconds. '*n*' represents the number of cortical patches analysed for the indicated strains under the adequate conditions to visualize RFP and mCherry or GFP. '*P*' represents *P*-value of the Student's *t*-test, compared with the isogenic wt. *P*-values under 0.001 indicate statistically significant differences. ND denotes not determined.

the individual IQ motifs or the *cmd1-231* mutation did not have any significant effect on the Myo5 dynamics (Table I).

Next, we investigated whether Cmd1 dissociation promoted early arrival of Myo5 to the endocytic sites and/or slowed down its dissociation from the PM. For this purpose, we examined the dynamics of long-lived (lifespan longer than 16 s) GFP-Myo5 patches relative to Sla1, in the *cmd1-226* mutant. The lifespan of the Sla1-mCherry was unaltered in the subpopulation of long-lived GFP-Myo5 patches (Table II, lifespan Sla1-mCherry, SCMIG1077 p*GFP-MYO5* versus SCMIG1078 p*GFP-MYO5*). However, the myosin arrived on average 5.5 s earlier in the *cmd1-226* mutant, as compared with the *CMD1* strain (Table II, t_a GFP-Myo5 and Figure 5). This result indicated that Cmd1 dissociation increased the probability of Myo5 meeting available binding partners at cortical patches. Interestingly also, GFP-Myo5 remained at the PM for a longer time (5.7 s on average) after departure of the endocytic coat in the *cmd1-226* mutant (Table II, t_d GFP-Myo5 and Figure 5). This observation suggested that Cmd1 reassociation to Myo5 might contribute to bring back the cortical myosin to the cytosol after vesicle fission occurs.

Cmd1 dissociation from Myo5 triggers actin polymerization in vitro and the assembly of actin at endocytic sites in vivo

Vrp1 is required to drive Myo5-induced actin polymerization (Geli *et al*, 2000; Lechler *et al*, 2001; Sun *et al*, 2006). Thus, we next investigated whether Cmd1 might also modulate the capacity of the Myo5 C_{ext} to trigger the assembly of endocytic actin structures. We have previously demonstrated that the Myo5 C_{ext} fused to GST and immobilized on the surface of glutathione-Sepharose beads induces the formation of complex actin structures in the presence of yeast extracts (Geli *et al*, 2000; Idrissi *et al*, 2002). The actin structures can be labelled with proteins involved in the endocytic uptake and its assembly requires the presence of Vrp1 and the Arp2/3 complex (Geli *et al*, 2000; Idrissi *et al*, 2002). PA-tagged Myo5 fragments containing either the C_{ext} alone (PA-C) or together with either the TH1 domain (PA-TC) or the neck and the TH1 domains (PA-nTC) were purified from yeast and immobilized on the surface of IgG-Sepharose beads. Similar to GST-C, PA-C induced assembly of actin structures, which could be visualized under the fluorescence microscope using rhodamine-labelled actin (Figure 6A). The structures could be labelled with the endocytic protein Abp1 (Figure 6A), and their formation was dependent on the presence of functional Vrp1 and Arp2/3 complex (Figure 6B). Consistent with the observation that the TH1 domain prevented binding of the C_{ext} to Vrp1 (Figure 2A), the presence of the TH1 domain (PA-TC) completely abolished the capacity of the Myo5 C_{ext} to induce the formation of actin patches (Figure 6C). Consistent with the hypothesis that Cmd1 dissociation might regulate this autoinhibitory interaction, we found that the construct bearing the neck (PA-nTC) could induce formation of the *in vitro* generated actin structures, only when it was purified under conditions that dissociated Cmd1 from the neck (5 mM $CaCl_2$; Figure 6C). The neck was required to promote calcium-induced actin polymerization in the presence of the TH1 domain as the $CaCl_2$ treatment did not alter the actin polymerization promoting capacity of PA-TC (Figure 6C). Finally, actin polymerization induced by Cmd1 dissociation was triggered by the C_{ext} as PA-nT failed to trigger the formation of actin patches under any of the experimental conditions assayed (Figure 6C).

Live-cell imaging of Abp1-RFP in strains bearing myosin-I mutations revealed that these molecular motors, together with Las17, have an essential function in promoting the assembly of complex actin structures at endocytic sites (Sun *et al*, 2006; Galletta *et al*, 2008). To investigate whether Cmd1 dissociation from Myo5 might regulate the assembly of the Abp1-containing actin structures *in vivo*, the dynamics of Abp1-RFP was analysed under conditions that disrupted the Myo5/Cmd1 interaction. In contrast to Sla1-mCherry, the Abp1-RFP lifespan at the endocytic patches was significantly

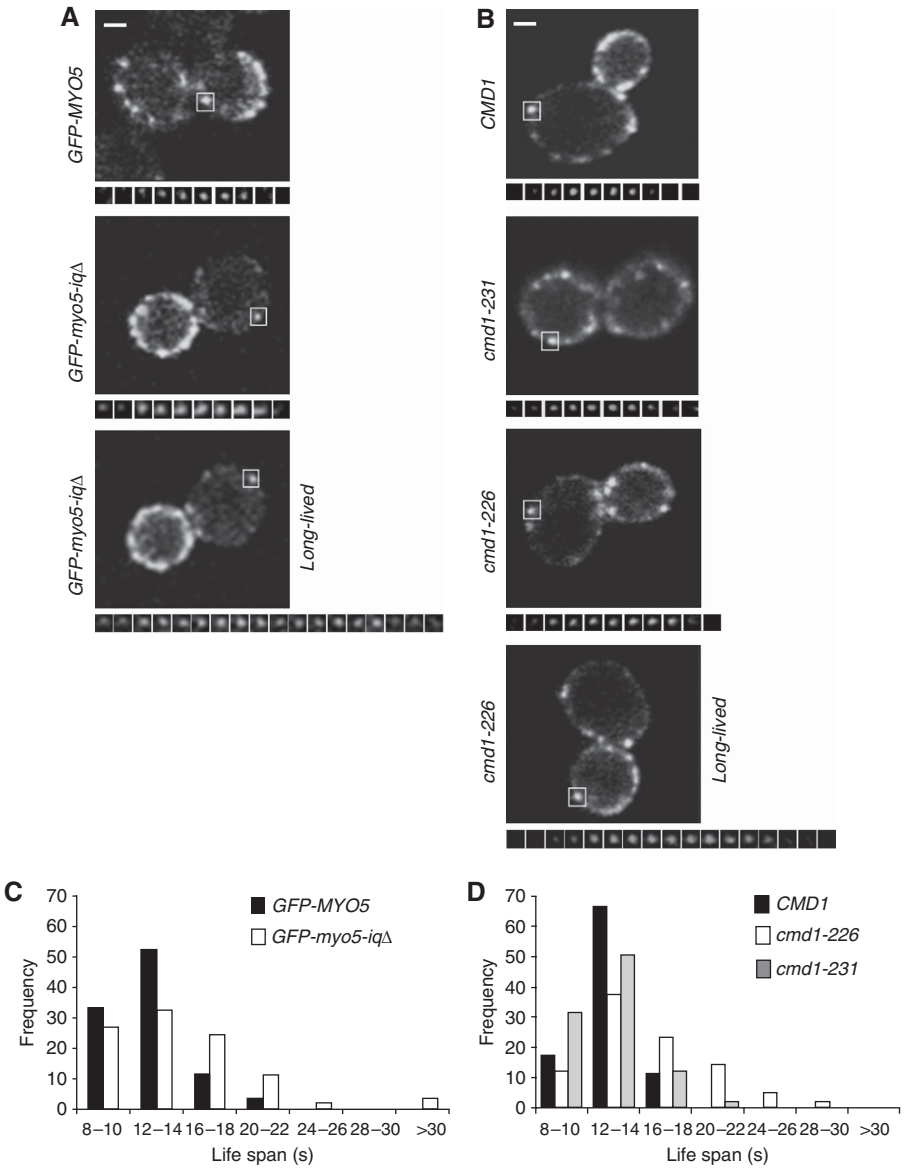

Figure 4 Cmd1 dissociation from Myo5 expands its lifespan at cortical patches. (**A**, **B**) Fluorescence micrographs of consecutive frames from time-lapse movies of cortical patches (lower panels) of GFP-Myo5 or GFP-Myo5-iqΔ, expressed in a *myo5*Δ strain (Y06549) (**A**) or GFP-Myo5 expressed in a *cmd1*Δ *myo5*Δ strain, expressing the wt *CMD1* (SCMIG1057) or the *cmd1-231* (SCMIG1059) or *cmd1-226* (SCMIG1058) mutants (**B**). The upper panels show a single frame of the imaged cells. The white square frames the cortical patch under analysis. Frames were recorded every 2 s. Constructs were expressed on centromeric plasmids under the *MYO5* promoter. (**C**, **D**) Frequency distribution for the lifespan of the 80 GFP-Myo5 cortical patches analysed for the strains described in (**A**, **B**), respectively. Bar = 1 μm.

Table II GFP-Myo5 arrives earlier to and departs later from the endocytic sites in the *cmd1-226* mutant

Strain Parameter	*CMD1 GFP-MYO5 SLA1-mCherry* (SCMIG1077 p*GFP-MYO5*)			*cmd1-226 GFP-MYO5 SLA1-mCherry* (SCMIG1078 p*GFP-MYO5*)			*P*
	Avg	s.d.	*n*	Avg	s.d.	*n*	
Ls Sla1-mCherry	26.0	3.3	20	24.9[a]	4.6[a]	20	0.3889
Ls GFP-Myo5	13.1	2.2	20	23.8[a]	4.6[a]	20	1×10^{-5}
t_a GFP-Myo5	17.7	4.0	20	12.3[a]	4.6[a]	20	2.5×10^{-4}
t_d GFP-Myo5	4.8	2.9	20	10.5[a]	3.7[a]	20	1×10^{-5}

Lifespans (Ls) of 20 correlative Sla1-mCherry and GFP-Myo5 patches and arrival (t_a) and departure times (t_d) of GFP-Myo5 relative to Sla1-mCherry, analysed in the indicated strains (see Materials and methods and Figure 5). The average (avg) and standard deviation (s.d.) are indicated in seconds. '*n*' represents the number of pairs of cortical patches analysed for the indicated yeast strains. '*P*' represents the *P*-value of the Student's *t*-test. *P*-values under 0.001 indicate statistically significant differences.
[a]Subpopulation associated with GFP-Myo5 cortical patches with lifespans longer than 16 s.

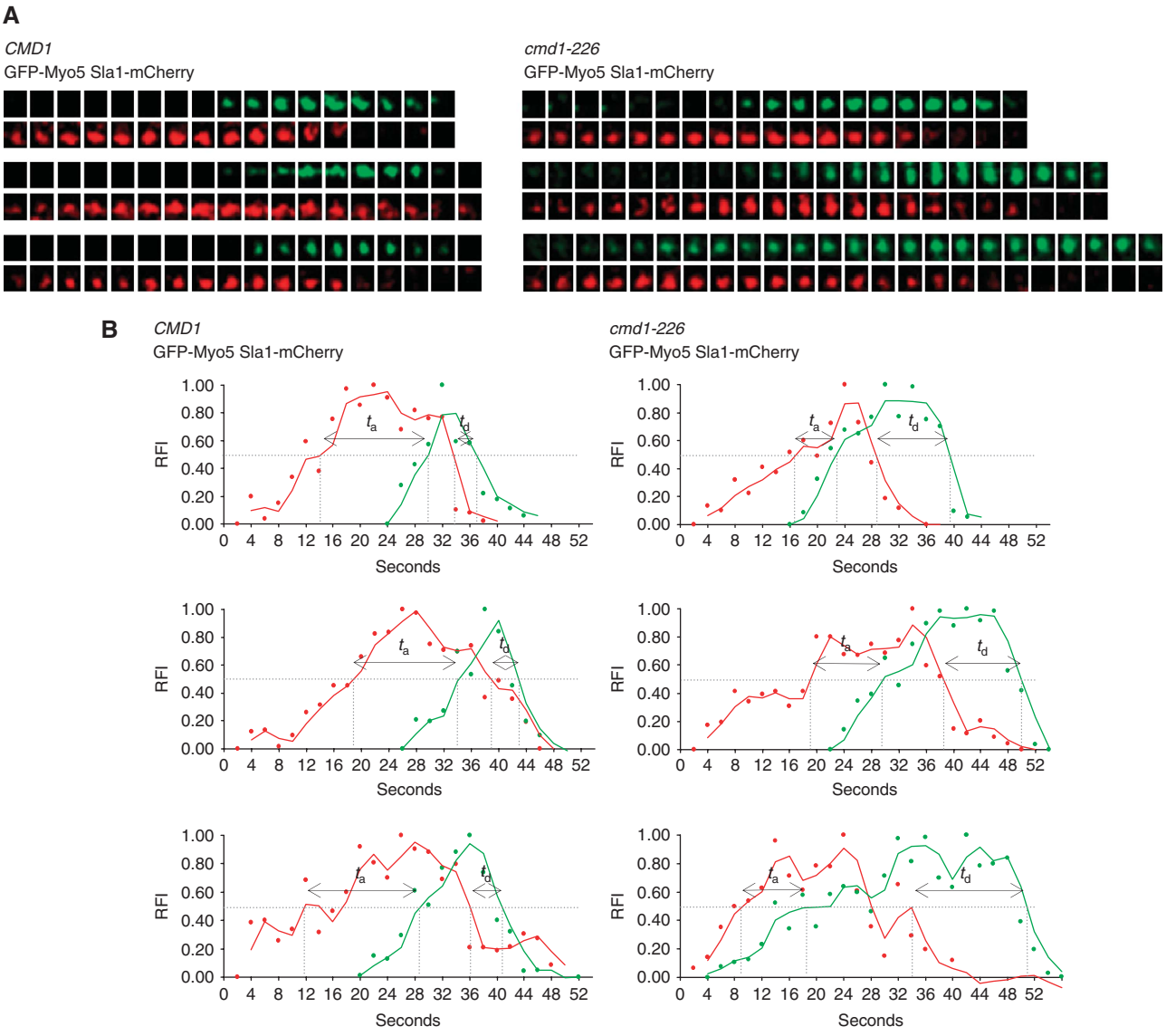

Figure 5 GFP-Myo5 arrives earlier to and departs later from the endocytic sites in the *cmd1-226* mutant. (**A**) Fluorescence micrographs of consecutive frames from three representative double-colour time-lapse movies of cortical patches in *cmd1*Δ *myo5*Δ strains with mCherry-tagged *SLA1*, expressing GFP-Myo5 from a centromeric plasmid under the *MYO5* promoter and either the wt *CMD1* (SCMIG1077) or the *cmd1-226* mutant (SCMIG1078). Frames were recorded every 2 s. GFP-Myo5 patches with lifespans longer than 16 s were analysed for the *cmd1-226* strain. (**B**) Graphs demonstrating the relative fluorescence intensity (RFI) plotted against time for the Sla1-mCherry (red) and GFP-Myo5 (green) double-colour time-lapse movies shown in (**A**). t_a and t_d indicate the arrival and departure times of GFP-Myo5 relative to Sla1-mCherry, respectively.

expanded in cells expressing the Myo5-iqΔ or the Cmd1-226 mutants, as compared with the isogenic wts (Table I, SCMIG880 p*GFP-MYO5* versus SCMIG880 p*GFP-myo5-iq*Δ and SCMIG1063 p*GFP-MYO5* versus SCMIG1064 p*GFP-MYO5*, RFP channel). When considering the subpopulation of GFP-Myo5 patches with lifespans longer than 16 s in the *cmd1-226* mutant, no significant differences were observed in the arrival time of GFP-Myo5 relative to Abp1-RFP, as compared with the isogenic wt (Table III, t_a GFP-Myo5 and Figure 7). Abp1-RFP recruitment closely followed Myo5 recruitment in both strains (Table III, t_a GFP-Myo5 and Figure 7). As Myo5 arrived earlier at the endocytic sites in the *cmd1-226* mutant (Table II, t_a GFP-Myo5 and Figure 5), the results indicated that Cmd1 dissociation from Myo5 favoured early arrival of Myo5 followed by early onset of actin polymerization. On the other hand, consistent with the observation that Abp1 travels into the cytosol together with the clathrin coat, Myo5 dissociation from the PM was delayed on average 5 s after departure of Abp1-RFP in the *cmd1-226* strain (Table III, t_d GFP-Myo5 and Figure 7; and Table II, t_d GFP-Myo5 and Figure 5).

Differential binding of cytosolic and PM-associated Myo5 to Cmd1 and Vrp1

Our data indicated that disruption of the Myo5/Cmd1 interaction promotes Myo5 binding to Vrp1, expands the myosin lifespan at cortical patches and activates myosin-I-induced actin polymerization *in vitro* and *in vivo*. Thus, the results strongly suggested that a mechanism involving Cmd1 dissociation from Myo5 regulates its recruitment and activity

at endocytic sites. If this hypothesis was correct, the PM-associated and cytosolic Myo5 should reciprocally bind Cmd1 and Vrp1.

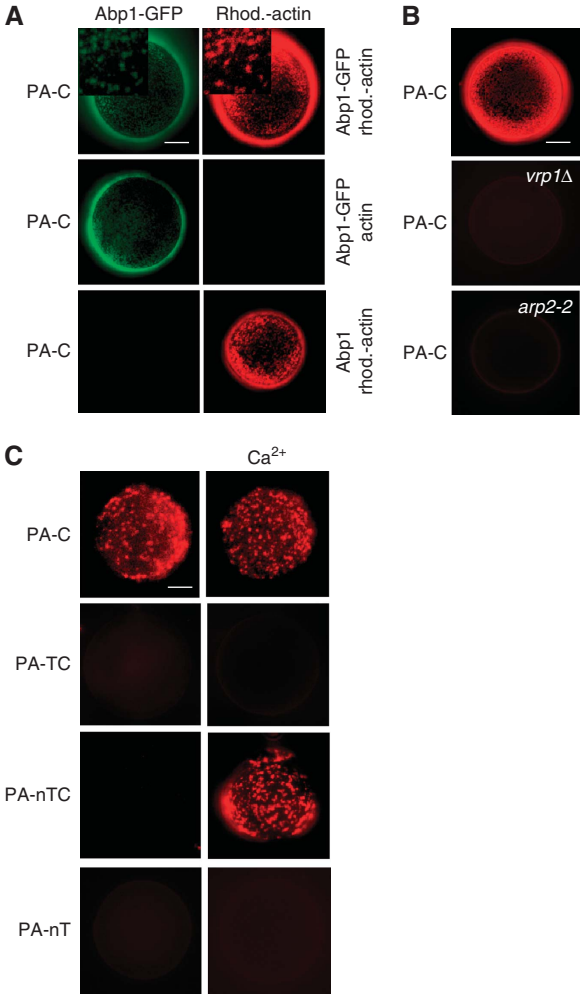

Figure 6 Cmd1 dissociation from Myo5 triggers actin polymerization *in vitro*. (**A–C**) Fluorescence micrographs of IgG-Sepharose beads coated with equimolar amounts of the indicated PA-Myo5 constructs incubated for 5 min at 26°C in the presence of yeast extracts from either *abp1*Δ strains, expressing Abp1-GFP (Y071BP19 p*ABP1-GFP*) or untagged Abp1 (Y071BP19 p*ABP1*) (**A**), wt (SCMIG19), *vrp1*Δ (SCMIG40) or *arp2-2* (HR4156) strains (**B**) or a wt strain (BY4741) (**C**), and 1 μM rhodamine-labelled actin (**A**, rhod.-actin, **B**, **C**) or unlabelled actin (**A**, actin) . Insets show higher magnifications of the Abp1-GFP and rhodamine-actin patches. Bar = 10 μm.

To test our hypothesis, we prepared cytosolic (C) and PM fractions from yeast cells expressing PA-Myo5 and analysed the amount of Cmd1 coprecipitating with the myosin-I in IgG-Sepharose pull downs. The GPI-anchored protein Gas1 and hexokinase (Hxk1) were used as PM and cytosolic markers, respectively (Figure 8A and C). As shown in Figure 8B, the PM-associated Myo5 (PM) clearly coprecipitated much less Cmd1 than the cytosolic Myo5 (C). The associated Cmd1 specifically bound to the Myo5 neck as the signal disappeared when PA-Myo5-iqΔ was used instead of the wt (Figure 8B). The lack of association of Myo5 with Cmd1 at the PM was not merely due to the low concentration of Cmd1 in this fraction (Figure 8A), as a 1 to 10 dilution of the cytosol did not alter binding of the cytosolic Myo5 to Cmd1 (C_{dil}; Figure 8B).

We next precipitated PA-Myo5 with IgG-Sepharose from cytosolic and PM fractions of yeast cells expressing Vrp1-HA (Figure 8C). As shown in Figure 8D, the PM-associated Myo5 (PM) coprecipitated much more Vrp1-HA than the cytosolic myosin (C). Vrp1 specifically bound to the PM-associated Myo5 as deletion of the C_{ext} (PA-HnT) completely eliminated Vrp1 from the precipitates (Figure 8D). The experiments indicated that, compared with the cytosolic Myo5, the PM-associated Myo5 is poorly bound to Cmd1 but strongly interacts with Vrp1. Consistent also with previous immunolocalization results (Brockerhoff and Davis, 1992), which failed to demonstrate the presence of Cmd1 at actin patches, we did not observe colocalization of Cmd1-mCherry and GFP-Myo5 at endocytic sites in live cells (Supplementary Figure S4). In contrast, Myo5 and Vrp1 overlap for 10 to 15 s at endocytic patches in analogous experiments (Sun *et al*, 2006).

Discussion

On the basis of our observations and the available literature, we propose the model depicted in Figure 9. According to this model, the cytosolic myosin bound to Cmd1 maintains a closed conformation where the TH1 domain interacts with the C_{ext} preventing association with Vrp1 and Myo5-induced actin polymerization. At the PM, a still unidentified mechanism releases the tight calmodulin/myosin-I interaction. As a consequence, the intramolecular inhibitory interaction is disrupted, allowing Myo5 binding to Vrp1 and local activation of Myo5-induced actin polymerization. Finally, Cmd1 reassociation to Myo5 contributes to dissociate it from the PM after vesicle fission.

Table III Early arrival of GFP-Myo5 to the endocytic sites in the *cmd1-226* is accompanied by early recruitment of Abp1-RFP

Strain	*CMD1 GFP-MYO5 Abp1-RFP* (SCMIG1063 p*GFP-MYO5*)			*cmd1-226 GFP-MYO5 Abp1-RFP* (SCMIG1064 p*GFP-MYO5*)			*P*
Parameter	Avg	s.d.	*n*	Avg	s.d.	*n*	
Ls Abp1-RFP	13.5	2.5	20	20.7[a]	5.2[a]	20	4×10^{-4}
Ls GFP-Myo5	11.7	1.9	20	24.3[a]	5.2[a]	20	2×10^{-6}
t_a GFP-Myo5	−0.05	2.8	20	−0.08[a]	3.4[a]	20	0.6436
t_d GFP-Myo5	−1.9	2.4	20	3.5[a]	4.25[a]	20	4×10^{-3}

Lifespans (Ls) of 20 correlative Abp1-RFP and GFP-Myo5 patches and arrival (t_a) and departure times (t_d) of GFP-Myo5 relative to Abp1-RFP, analysed in the indicated strains (see Materials and methods and Figure 7). The average (avg) and standard deviation (s.d.) are indicated in seconds. '*n*' represents the number of pairs of cortical patches analysed for the indicated yeast strains. '*P*' represents the *P*-value of the Student's *t*-test. *P*-values under 0.001 indicate statistically significant differences.
[a]Subpopulation associated with GFP-Myo5 cortical patches with lifespans longer than 16 s.

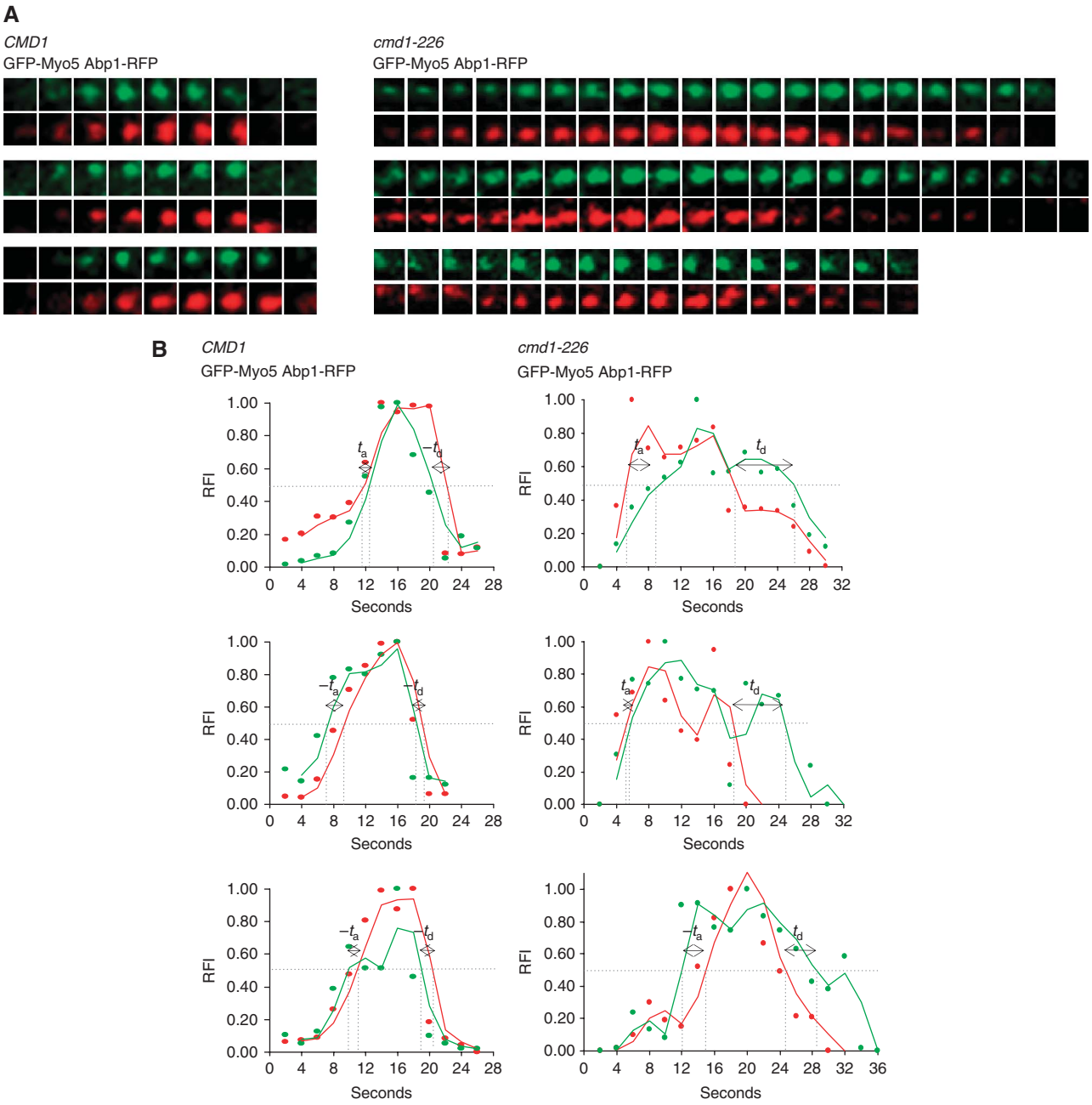

Figure 7 Cmd1 dissociation from Myo5 triggers actin assembly at endocytic sites. (**A**) Fluorescence micrographs of consecutive frames from double-colour time-lapse movies of three representative cortical patches in *cmd1*Δ *myo5*Δ strains with RFP-tagged *ABP1*, expressing GFP-Myo5 from a centromeric plasmid under the *MYO5* promoter and either the wt *CMD1* (SCMIG1063) or the *cmd1-226* mutant (SCMIG1064). Frames were recorded every 2 s. GFP-Myo5 patches with lifespans longer than 16 s were analysed for the *cmd1-226* strain. (**B**) Graphs demonstrating the relative fluorescence intensity (RFI) plotted against time for the Abp1-RFP (red) and GFP-Myo5 (green) double-colour time-lapse movies shown in panel (**A**). t_a and t_d indicate the arrival and departure times of GFP-Myo5 relative to ABP1-RFP, respectively.

Robust evidence for a direct intramolecular interaction between the myosin TH1 domain and the C_{ext} was already present in the literature for the long-tailed protozoal myosins-I. Similar to what we found for Myo5, pull-down experiments with purified components demonstrated such interaction for the *Acanthamoeba castellanii* myosin-IA (Lee *et al*, 1999). In addition, structural data on the *A. castellanii* myosin-IB and C showed a surprising globular structure of the tail, where the SH3 domain folds back on the TH1 domain (Jontes *et al*, 1998; Ishikawa *et al*, 2004). More recently, Hwang *et al* (2007) have provided NMR data supporting such an intramolecular interaction. We have now revealed the physiological significance of this interaction and described a molecular mechanism that might contribute to its modulation.

We showed that the TH1 domain prevented interaction of the Myo5 C_{ext} with Vrp1 in immunoprecipitation experiments. Consistent with the cellular function described for the Myo5/Vrp1 interaction (Anderson *et al*, 1998; Geli *et al*, 2000; Lechler *et al*, 2001; Sun *et al*, 2006), we also found that the TH1 domain impairs recruitment of the Myo5 C_{ext} to cortical patches *in vivo* and abrogated its activity as an actin polymerization promoting factor *in vitro*. The TH1 domain most likely exerted its inhibitory activity intramolecularly, as we failed to demonstrate oligomerization of the myosin

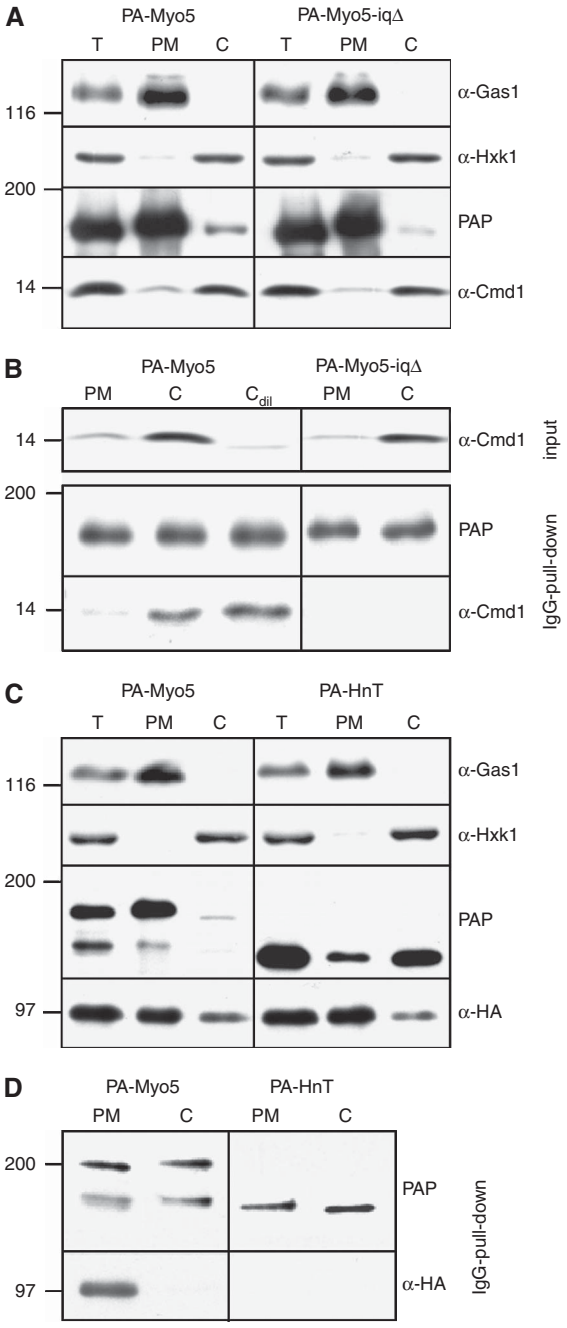

Figure 8 Differential binding of cytosolic and PM-associated Myo5 to Cmd1 and Vrp1. (**A**, **C**) Immunoblots of 10 μg of total (T), PM or cytosolic (C) fractions prepared from *myo5*Δ cells (SCMIG275) (**A**) or *myo5*Δ *vrp1*Δ cells (SCMIG304) expressing Vrp1-HA (**C**), expressing the indicated PA-Myo5 constructs. PAP, a peroxidase-conjugated anti-HA antibody and antibodies against Cmd1 or the PM and cytosolic markers Gas1 and Hxk1, combined with the appropriate peroxidase-conjugated secondary antibody, were used for detection of the PA-Myo5 constructs, Vrp1-HA, Cmd1, Hxk1 or Gas1, respectively. (**B**, **D**) Immunoblots of IgG pull downs from yeast PM and cytosolic (C) fractions from *myo5*Δ cells (SCMIG275) (**B**) or *myo5*Δ *vrp1*Δ cells (SCMIG304) expressing Vrp1-HA (**D**), expressing the indicated PA-Myo5 constructs. Membranes were processed as described in (**A**, **C**).

under the same experimental conditions that showed the Myo5/Vrp1 and Myo5/Cmd1 interactions (Supplementary Figure S5).

An autoinhibitory activity contained within the TH1 domain was not described before. On the contrary, the TH1

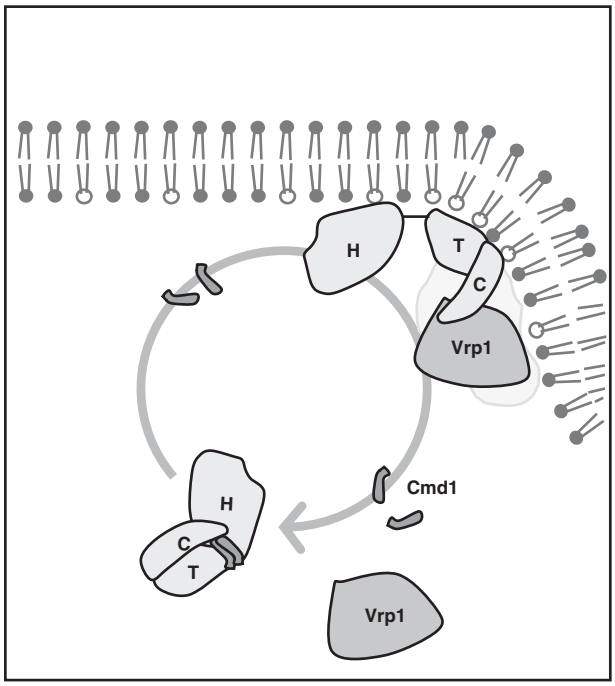

Figure 9 A model for the regulation of Myo5 recruitment and activation at the cortical endocytic patch. Cytosolic Myo5 interacts with Cmd1, which stabilizes a conformation where the C_{ext} (C) folds back and binds to the TH1 (T) domain. Under this circumstance, the SH3 domain is not accessible for binding to Vrp1. An intracellular signal at the PM causes Cmd1 dissociation from the Myo5 neck and releases the inhibitory interaction. SH3-mediated binding of Myo5 to Vrp1 concentrates Myo5 at the cortical endocytic patches and triggers Myo5-induced actin polymerization. Cmd1 reassociation to the Myo5 neck contributes to dissociate it from the PM.

domain has been shown to bind acidic phospholipids (Adams and Pollard, 1989; Hayden *et al*, 1990; Doberstein and Pollard, 1992) and to contribute to membrane targeting of different myosins-I (Miyata *et al*, 1989; Lee *et al*, 2000; Yamashita *et al*, 2000; Oberholzer *et al*, 2004). The TH1 domain of Myo5 also binds to acidic phospholipids (data not shown) and its deletion causes partial mislocalization of the myosin to the cytosol (Figure 1; GFP-HnC). Thus, in addition to the autoinhibitory activity, the TH1 domain probably exerts a positive function by recruiting Myo5 to the inner leaflet of the PM.

On the other hand, our work also revealed that Cmd1 dissociation promoted Myo5 binding to Vrp1. Again in agreement with previously published data on the function of the Myo5/Vrp1 interaction (Anderson *et al*, 1998; Geli *et al*, 2000; Lechler *et al*, 2001; Jonsdottir and Li, 2004; Sun *et al*, 2006), we found that dissociation of Cmd1 from Myo5 significantly extended the myosin lifespan at cortical patches, enhanced actin polymerization at endocytic sites and triggered Myo5-induced actin polymerization *in vitro*. Concomitantly, Cmd1 dissociation weakened the interaction between a fragment containing the neck and TH1 domains and the C_{ext}. Considering all the data, it is reasonable to propose that Cmd1 dissociation promotes Myo5 binding to Vrp1 by releasing the autoinhibitory interaction between the TH1 domain and the C_{ext}.

We made the novel observation that the Cmd1-bound but not the Cmd1-stripped Myo5 neck strongly interacts with the C_{ext} and most likely contributes to stabilize the inhibitory

interaction between the adjacent TH1 domain and the C_{ext} (Figure 2C; Supplementary Figure S3A). On the basis of the Myo5 IQ motifs sequences, it appears likely that Cmd1 is bound in an extended conformation (Terrak *et al*, 2005), with one lobe free to interact with the C_{ext}. Thus, it is tempting to propose a simple model where Cmd1 works as a clamp that holds the TH1 domain folded onto the C_{ext}. However, our results indicated that the activation mechanism might have a second level of complexity. On the one hand, we failed to detect a direct interaction between free Cmd1 and the C_{ext} (Supplementary Figure S3B and C). This raises the interesting possibility that Cmd1 might need to interact first to the Myo5 neck in order to cross-link the nT and C fragments. On the other hand, our results suggested that the presence of an intact neck is important to release the autoinhibitory interaction when the TH1 is covalently linked to the C_{ext}. This was inferred from the observation that deletion of the neck in the presence of the TH1 domain completely abolished C_{ext}-dependent recruitment of Myo5 to cortical patches, Myo5 interaction with Vrp1 and Myo5-induced actin polymerization. Deletion of the neck might cause missfolding of the tail, thereby preventing Vrp1 association. However, this is probably not the case because the HTC construct binds to Rvs167 similar to the wt Myo5 (Figure 2B) and partial Trypsin digestion experiments indicated an analogous conformation for the Cmd1-bound wt Myo5 and for the HTC mutant (Supplementary Figure S6, see below). Further evidence supporting the active function of the neck in releasing the autoinhibition derives from the Myo5-iqΔ mutant. We found that this Myo5 mutant, which lacks a portion of the neck, was less efficient than the *cmd1-226* mutant in extending the Myo5 lifespan at cortical sites and in promoting Myo5 binding to Vrp1.

Interestingly, a major conformational change induced in the TH1 domain of the short-tailed Brush Border myosin-I can be observed upon calmodulin dissociation from the myosin neck (Whittaker and Milligan, 1997). We hypothesize that dissociation of Cmd1 could transmit a conformational change from the neck to the TH1 domain, which could influence its affinity for the C_{ext}. Consistent with this view, we have found that Cmd1 dissociation was accompanied by the exposure of a Trypsin digestion site within the TH1 domain and that exposure of this additional site required the presence of an intact neck (Supplementary Figure S6). Thus, treatment of the wt Myo5 with 5 mM $CaCl_2$ exposed a Trypsin digestion site that generated an N-terminal 116 kDa fragment (Supplementary Figure S6, Myo5 Cmd1, $CaCl_2$). This fragment was also present after digestion of the wt Myo5 purified from the *cmd1-226* mutant, independently of the presence of $CaCl_2$ (Supplementary Figure S6). The Trypsin digestion site seemed to be less exposed in the Myo5-iqΔ mutant and it could not be detected in the HTC construct, which lacks the complete neck (Supplementary Figure S6). Alternatively or in addition to a putative conformational change transmitted from the neck to the TH1 domain, the Cmd1-stripped neck could bind other molecules that sterically hinder the TH1/C_{ext} interaction (Swanljung-Collins and Collins, 1992; Cyr *et al*, 2002; Tang *et al*, 2002; Hirono *et al*, 2004; Phillips *et al*, 2006) or it might recruit enzymes that modify the Myo5 tail.

Intramolecular interactions regulating protein localization and function of a number of factors that promote actin polymerization have been described before. An interaction between the N- and C-terminus of the mammalian formin formin-related gene in leukocytes α (FRLα) modulates its PM localization and actin assembly activity (Seth *et al*, 2006). Similarly, induction of Arp2/3 complex-dependent actin polymerization by the C-terminal portion of neuronal WASP is autoinhibited by the N-terminal fragment (Rohatgi *et al*, 2000). Local activation of actin polymerization promoting factors can be achieved by direct interaction with signal transducers such as Cdc42 and $PIns(4,5)P_2$, which release the autoinhibitory interactions (Rohatgi *et al*, 2000; Seth *et al*, 2006). Downregulating futile cycles of actin polymerization might be essential to prevent energy waste and the assembly of actin structures that could interfere with a number of cellular functions.

A key question that follows from our work is the nature of the signal triggering Cmd1 release and activation of Myo5 at endocytic sites. Even though increasing evidence points to a function of calcium and calmodulin regulating endocytic uptake in mammals (Wu *et al*, 2009), we do not favour the idea that calcium triggers Cmd1 dissociation from Myo5 at endocytic sites because a Cmd1 mutant that does not bind calcium (*cmd1-3*) (Geiser *et al*, 1991) does not exhibit an uptake defect in yeast (Kubler *et al*, 1994). Nevertheless, further experiments would be required to rule out this possibility. On the contrary, a number of results indicate that local production of $PIns(4,5)P_2$ at endocytic sites could contribute to trigger Cmd1 dissociation from Myo5. First, it was recently shown that myosin-I mutants exhibit synthetic lethal interactions with mutations in the Mss4 PIns4P-5 kinase responsible for the production of $PIns(4,5)P_2$ at endocytic sites (Audhya *et al*, 2004). Further, the lifespan of Myo5 is significantly expanded in a yeast synaptojanin mutant defective in $PIns(4,5)P_2$ consumption (Sun *et al*, 2007). Finally, Hayden *et al* (1990) demonstrated that association of the Brush Border myosin-I with liposomes containing $PIns(4,5)P_2$ displaces calmodulin from the myosin neck. In addition, other molecular mechanisms including protein kinase C-dependent phosphorylation of the myosin-I neck and/or actin and nucleotide binding to the motor head (Lieto-Trivedi and Coluccio, 2008) might contribute to lower the tight myosin-I/calmodulin interaction. Further studies will now be required to investigate these possibilities.

Materials and methods

Strains and genetic techniques

Yeast strains used are listed in Table IV. Details on strain construction are available upon request. Strains without plasmids were grown in complete yeast peptone dextrose and strains with plasmids were selected on synthetic dextrose complete (SDC) lacking the appropriate nutrient (Dulic *et al*, 1991) at 25°C. Scoring of genetic markers was performed as described (Sherman *et al*, 1974). Transformation of yeast was accomplished by the lithium acetate method (Ito *et al*, 1983). All tagged versions of yeast genes used in this study complemented the growth defects of the corresponding knock-out strains.

DNA techniques and plasmid construction

Plasmids used are listed in Table V. Details on plasmid construction are available upon request. DNA manipulations were performed as described (Sambrook *et al*, 1989). Enzymes for molecular biology were obtained from New England Biolabs. Plasmids were purified with the *Nucleospin* plasmid purification kit (Macherey-Nagel). DNA was purified from agarose gels using the gel extraction kit from

Table IV Yeast strains

Strain	Genotype	Reference
SCMIG182	*MAT***a** *ade2 ade3::cmd1-226::TRP1 his3 leu2 lys2 trp1 ura3 cmd1Δ::HIS3 bar1Δ::LYS2*	Geli *et al* (1998)
SCMIG947	*MAT***a** *ade2 ade3::CMD1::TRP1 his3 leu2 lys2 trp1 ura3 cmd1Δ::HIS3 bar1Δ::LYS2*	Geli *et al* (1998)
SCMIG187	*MAT***a** *ade2 ade3:: cmd1-231::TRP1 his3 leu2 lys2 trp1 ura3 cmd1Δ::HIS3bar1::LYS2*	Geli *et al* (1998)
SCMIG19	*MAT***a** *his3 leu2 trp1 ura3 bar1*	Idrissi *et al* (2002)
SCMIG275	*MAT***a** *his3 leu2 lys2 trp1 ura3 bar1 myo5Δ::TRP1*	Idrissi *et al* (2002)
SCMIG40	*MAT***a** *vrp1Δ::URA3 ura3 leu2 his3 lys2 trp1 ade2 bar1*	Geli *et al* (2000)
RH4165	*MAT***a** *arp2-2::URA3 ura3 leu2 his3 trp1 ade2 bar1*	Idrissi *et al* (2002)
BY4741	*MAT***a** *leu2 his3 ura3 met15*	Euroscarf
Y06549	*MAT***a** *myo5Δ::KMX leu2 his3 ura3 met15*	Euroscarf
Y07199	*MAT***a** *abp1Δ::KMX leu2 his3 ura3 met15*	Euroscarf
SCMIG304	*MAT***a** *his3 leu2 lys2 trp1 ura3 bar1 vrp1Δ::URA3 myo5Δ::TRP1* + pURA3*MYO5*	Geli *et al* (2000)
SCMIG880	*MATα ura3 leu2 his3 trp1 myo5Δ::TRP1 ABP1-RFP::KMX bar1?*	This study
SCMIG1047	*MAT***a** *his3 leu2 trp1 ura3 met15 cmd1Δ::KMX myo5Δ::KMX pURA3CMD1*	This study
SCMIG1057	*MAT***a** *his3 leu2 trp1 ura3 met15 cmd1Δ::KMX myo5Δ::KMX pTRP1CMD1*	This study
SCMIG1058	*MAT***a** *his3 leu2 trp1 ura3 met15 cmd1Δ::KMX myo5Δ::KMX pTRP1 cmd1-226*	This study
SCMIG1059	*MAT***a** *his3 leu2 trp1 ura3 met15 cmd1Δ::KMX myo5Δ::KMX pTRP1 cmd1-231*	This study
SCMIG1061	*MAT***a** *his3 leu2 trp1 ura3 met15 cmd1Δ::KMX myo5Δ::KMX ABP1-RFP::KMX pURA3CMD1*	This study
SCMIG1063	*MAT***a** *his3 leu2 trp1 ura3 met15 cmd1Δ::KMX myo5Δ::KMX ABP1-RFP::KMX pTRP1CMD1*	This study
SCMIG1064	*MAT***a** *his3 leu2 trp1 ura3 met15 cmd1Δ::KMX myo5Δ::KMX ABP1-RFP::KMX pTRP1 cmd1-226*	This study
SCMIG1076	*MAT***a** *his3 leu2 trp1 ura3 met15 cmd1Δ::KMX myo5Δ::KMX SLA1-mCherry::HIS3MX pURA3CMD1*	This study
SCMIG1077	*MAT***a** *his3 leu2 trp1 ura3 met15 cmd1Δ::KMX myo5Δ::KMX SLA1-mCherry::HIS3MX pTRP1CMD1*	This study
SCMIG1078	*MAT***a** *his3 leu2 trp1 ura3 met15 cmd1Δ::KMX myo5Δ::KMX SLA1-mCherry::HIS3MX pTRP1 cmd1-226*	This study
SCMIG1079	*MAT***a** *myo5Δ::KMX leu2 his3 ura3 met15 SLA1-mCherry::HIS3MX*	This study
SCMIG1080	*MAT***a** *his3 leu2 ura3 met15 myo5Δ::KMX CMD1-mCherry::HIS3MX*	This study

Qiagen. Transformation of *E. coli* was performed by electroporation (Dower *et al*, 1988). PCRs were performed with a Vent polymerase (New England Biolabs) and a TRIO-thermoblock (Biometra GmbH). Oligonucleotides were synthesized by Interactiva.

SDS–PAGE, immunoblots and antibodies

SDS–PAGE was performed as described (Laemmli, 1970) using a minigel system (Bio-Rad Laboratories). High and low range SDS–PAGE molecular weight standards (Bio-Rad Laboratories) were used. Coomassie brilliant blue (Harlow and Lane, 1988) was used for detection of total protein. Protein concentration was determined with the Bio-Rad Protein Assay (Bio-Rad Laboratories). Immunoblots were performed as described (Geli and Riezman, 1998) except that transfer of Gas1 was done overnight in the absence of methanol. Antibodies used are listed in Table VI. Nitrocellulose membranes were stained with Ponceau Red for detection of total protein (Harlow and Lane, 1988). An enhanced chemoluminescence (ECL) detection kit (Amersham Biosciences) was used for detection of peroxidase-conjugated antibodies.

Protein purification from yeast and E. coli

Purification of recombinant GST fusion proteins from BL21 *E. coli* (Novagen) was performed as described (Geli *et al*, 2000). Cmd1 was released from the GST-Cmd1-coated glutathione-Sepharose beads by digestion with thrombin-agarose (Thrombin clean cleavage kit, Sigma). Glutathione-Sepharose beads were from Amersham Biosciences. PA-nT was purified from SCMIG275 pPA-nT using IgG-Sepharose (Amersham-Bioscience). After glass bead-lysis in 100 μl of IP buffer (50 mM Tris, pH 7.5, 150 mM NaCl, 5 mM EDTA) in the presence of protease inhibitors (PIs) (0.5 mM PMSF, 1 μg/ml aprotinin, 1 μg/ml pepstatin, 1 μg/ml leupeptin, 1 μg/ml antipain), NaCl and Triton X-100 were adjusted to 0.5 M and 1% final concentrations, respectively. Unbroken cells were eliminated by centrifugation at 2500 *g* for 5 min. After centrifugation at 10 000 *g* for 10 min at 4°C, the supernatant was incubated with IgG-Sepharose for 2 h at 4°C. Beads were collected and stepwise eluted with 20 μl of 0.5 M acetic acid pH 3.4 (adjusted with ammonium acetate), 0.5 M NaCl, 0.1% Tween-20. The eluate was mixed with 10 μl of 1 M Tris pH 9 for pH neutralization. For the purification of the Cmd1-free PA-nT, 5 mM $CaCl_2$ was added to the extract before addition of the Sepharose.

Overlay, pull downs and immunoprecipitations

For the glutathione-Sepharose pull downs, 1 μg of bead-bound GST-C or GST were incubated with 30 ng of PA-nT bound to Cmd1 or Cmd1-free PA-nT in 1 ml TBS-TB (10 mM Tris pH 8.0, 150 mM NaCl, 0.1% Tween-20, 1.5% BSA) for 3 h at 4°C. Where indicated, 5 mM $CaCl_2$ was added to promote Cmd1 dissociation and 1 μg of Cmd1 was added in the presence of 1 mM EGTA to promote reassociation. Beads were collected, washed with TBS-TB and TBS-T (10 mM Tris pH 8.0, 150 mM NaCl, 0.1% Tween-20) and eluted in SDS-sample buffer. For the IgG pull downs from yeast extracts, cells were glass bead-lysed in LB (25 mM Tris, pH 8.5, 5 mM EDTA) in the presence of PIs. Unbroken cells were eliminated at 700 *g* for 10 min at 4°C. The supernatant was diluted with the same volume of BB (10 mM Tris pH 7.5, 0.2 mM EDTA, 0.2 mM DTT) containing PIs. After centrifugation at 700 *g* for 10 min at 4°C, the extract was adjusted to 10 mg of protein/ml and Triton X-100 and NaCl were added to 1% and 150 mM final concentrations, respectively. A measure of 1 ml of extract was incubated with 30 μl of 50% IgG-Sepharose for 2 h at 4°C. Beads were washed with LB:BB (1:1), 1% Triton X-100, 150 mM NaCl, and subsequently with LB:BB (1:1) and boiled in 25 μl SDS-sample buffer. Four 1:2 dilutions were loaded for each construct and immunoblotted for PA and Vrp1-HA. The corresponding signals were compared within the linear range. Quantifications were performed with imageJ from at least three independent experiments. The Vrp1-HA signal was normalized to the PAP signal for each sample.

For IgG-Sepharose pull downs from PM and cytosolic fractions, 0.5 ml of the different fractions were diluted with 0.5 ml of LB:BB (1:1) in the presence of PIs. Triton X-100 and NaCl were added to 1% and 150 mM final concentration, respectively. Samples were incubated with 40 μl of 50% IgG-Sepharose for 2 h at 4°C. Beads were washed with LB:BB (1:1), 1% Triton X-100, 150 mM NaCl and eluted with 25 μl SDS-sample buffer.

For the overlay assay, 0.15 μg of the nT fragment was separated by SDS–PAGE and transferred to a nitrocellulose filter in 30 mM Tris, 240 mM Glycine. Proteins were then partially renaturated in 10 mM Tris pH 8, 150 mM NaCl, 0.05% Tween-20 and the membrane was blocked over night at 4°C in blocking buffer (10 mM Tris pH 8, 150 mM NaCl, 0.05% Tween-20, 3% BSA). The membrane was then overlaid with 20 mM purified GST, GST-C or 60 mM Cmd1 for 3 h at 4°C, then with the goat anti-GST antibody or the rabbit anti-Cmd1 for 1.5 h at 4°C and finally with a peroxidase-conjugated antibody against goat IgG for 1 h in blocking buffer. After washing with blocking buffer and subsequently with 10 mM Tris pH 8, 150 mM NaCl, 0.05% Tween-20, peroxidase was detected with an ECL detection kit. For excision of the nT fragment from the PA-nT-coated beads, the PA-nT-coated IgG-Sepharose beads were incubated in 30 μl of 50 mM Tris pH 8, 0.5 mM EDTA and 10 Units (1 μl) of AcTEV (Invitrogen) over night at 4°C. The supernatant was discarded and the protein, which was still bound to the Sepharose beads, was eluted by incubating in 30 μl of 50 mM Tris pH 8, 1 M NaCl, 0.5 mM EDTA for 30 min with shaking at 4°C.

Table V Plasmids

Plasmid	Marker	Ori	Insert	Reference
p*MYO5*	*URA3*	*CEN4*	*MYO5*	Geli and Riezman (1996)
pHTC	*URA3*	*CEN4*	*myo5* (aa 1–1219)–(aa 705–773)Δ	This study
pHnC	*URA3*	*CEN4*	*myo5* (aa 1–1219)–(aa 774–905)Δ	This study
p*mycMYO5*	*LEU2*	*CEN4*	*myc-MYO5*	This study
p*MYO5-HA3*	*URA3*	*CEN4*	*MYO5* + *3HA*	Idrissi *et al* (2002)
pGEX-5X-3	—	—	GST	Pharmacia
pGST-C	—	—	*GST-myo5* (aa 982–1219)	Geli *et al* (2000)
p*GST-CMD1*	—	—	*GST-CMD1*	This study
p*GFP-MYO5*.LEU	*LEU2*	*CEN4*	*GFP-MYO5*	This study
p*GFP-MYO5*	*URA3*	*CEN4*	*GFP-MYO5*	This study
p*GFP-myo5-iq*Δ	*URA3*	*CEN4*	*GFP-myo5* (aa 1–1219)–(aa 725–735)Δ (aa 743–753)Δ	This study
p*GFP-myo5-iq1*Δ	*URA3*	*CEN4*	*GFP-myo5* (aa 1–1219)–(aa 725–735)Δ	This study
p*GFP-myo5-iq2*Δ	*URA3*	*CEN4*	*GFP-myo5* (aa 1–1219)–(aa 743–753)Δ	This study
pGFP-H	*URA3*	*CEN4*	*GFP-myo5* (aa 1–704)	This study
pGFP-Hn	*URA3*	*CEN4*	*GFP-myo5* (aa 1–773)	This study
pGFP-HnT	*URA3*	*CEN4*	GFP-*myo5* (aa 1–996)	This study
pGFP-HTC	*URA3*	*CEN4*	*GFP-myo5* (aa 1–1219)–(aa 705–773)Δ	This study
pGFP-HnC	*URA3*	*CEN4*	*GFP-myo5* (aa 1–1219)–(aa 774–905)Δ	This study
pGFP-nT	*URA3*	*CEN4*	*GFP-myo5* (aa 705–996)	This study
pGFP-nTC	*URA3*	*CEN4*	*GFP-myo5* (aa 705–1219)	This study
pGFP-TC	*URA3*	*CEN4*	*GFP-myo5* (aa 774–1219)	This study
pGFP-C	*URA3*	*CEN4*	*GFP-myo5* (aa 882–1219)	This study
pGFP-HC	*URA3*	*CEN4*	*GFP-myo5* (aa 705–905)Δ	This study
p*ABP1-GFP*	*URA3*	*CEN4*	*ABP1-GFP*	This study
p*ABP1*	*URA3*	*CEN4*	*ABP1-GFP*	This study
p*VRP1-GFP*	*LEU2*	*CEN4*	*VRP1-GFP*	This study
p*PA-MYO5*	*URA3*	*CEN4*	*Protein A-MYO5*	This study
p*PA-myo5-iq*Δ	*URA3*	*CEN4*	*Protein A-myo5* (aa 1–1219)–(aa 725–735)Δ (aa 743–753)Δ	This study
p*PA-myo5-iq1*Δ	*URA3*	*CEN4*	*Protein A-myo5* (aa 1–1219)–(aa 725–735)Δ	This study
p*PA-myo5-iq2*Δ	*URA3*	*CEN4*	*Protein A-myo5* (aa 1–1219)–(aa 743–753)Δ	This study
pPA-H	*URA3*	*CEN4*	*Protein A-myo5* (aa 1–704)	This study
pPA-Hn	*URA3*	*CEN4*	*Protein A-myo5* (aa 1–773)	This study
pPA-HnT	*URA3*	*CEN4*	*Protein A-myo5* (aa 1–996)	This study
pPA-HTC	*URA3*	*CEN4*	*Protein A-myo5* (aa 1–1219)–(aa 705–773)Δ	This study
pPA-HnC	*URA3*	*CEN4*	*Protein A-myo5* (aa 1–1219)–(aa 774–905)Δ	This study
pPA-nT	*URA3*	*CEN4*	*Protein A-myo5* (aa 705–996)	This study
pPA-nTC	*URA3*	*CEN4*	*Protein A-myo5* (aa 705–1219)	This study
pPA-TC	*URA3*	*CEN4*	*Protein A-myo5* (aa 774–1219)	This study
pPA-C	*URA3*	*CEN4*	*Protein A-myo5* (aa 882–1219)	This study
pPA-HT	*URA3*	*CEN4*	*Protein A-myo5* (aa 1–996)–(aa 705–773)Δ	This study
p*VRP1-HA*	*LEU2*	*CEN4*	*VRP1* + 3HA	This study
p*LexA-RVS167*	*HIS3*	2 μ	*LexA* + *RVS167*	This study
pLexA-nT	*HIS3*	2 μ	*LexA* + *myo5* (aa 705–996)	This study
pLexA-n	*HIS3*	2 μ	*LexA* + *myo5* (aa 705–773)	This study

Table VI Antibodies

Antigen	Source	Modification	Reference	Dilution
Peroxidase	Rabbit antibody	Peroxidase conjugated, peroxidase complex (PAP)	DAKO A/S	1:1000
Gas1	Rabbit serum		Muniz *et al* (2001)	1:50 000
Hxk1	Rabbit serum		van Tuinen and Riezman (1987)	1.2000
Cmd1	Rabbit serum		Geli *et al* (1998)	1:1000
HA	Rat monoclonal antibody (3F10)		Roche	1:1000
HA	Rat monoclonal antibody (3F10)	Peroxidase conjugated	Roche	1:500
MYC	Mouse monoclonal antibody (9E10)		Roche	1:2000
GST	Goat serum		Amersham Biosciences	1:2000
Rvs167	Rabbit		H. Riezman	1/10 000
LexA	Mouse monoclonal antibody		Santa Cruz	1:2000
GFP	Rabbit IgG		Invitrogen	1:1700
Mouse IgG	Goat antibody	Peroxidase conjugated	Sigma	1:4000
Rabbit IgG	Goat antibody	Peroxidase conjugated	Sigma	1:5000
Rat IgG	Goat antibody	Peroxidase conjugated	Sigma	1:5000
Goat IgG	Rat IgG	Peroxidase conjugated	Sigma	1:2000

For the pull-down experiments (Figure 2C), 1 μg of bead-bound GST-C or GST were incubated with protein extracts of the strains expressing PA-H, PA-Hn, PA-HT and PA-HnT prepared in IP buffer 1% Triton X-100 in the presence of PIs. After incubation for 1 h at 4°C, beads were recovered, washed three times with IP buffer 1% Triton X-100 and twice with IP buffer. Beads were resuspended in

30 μl of SDS-sample buffer and extracted proteins were separated by SDS–PAGE and transferred to a nitrocellulose filter. GST-C and GST were detected by staining with Ponceau red and the PA-Myo5 constructs were detected using PAP. In all, 1/125 of the total protein extracts were loaded as input.

Purification of yeast PM and cytosol

The isolation of PM and cytosolic fractions were performed based on (Serrano, 1988). For further detail see supplementary data.

In vitro actin polymerization assay

The rhodamine-actin polymerization assay on Sepharose beads was performed as described (Idrissi *et al*, 2002) except that IgG-Sepharose beads coated with PA-tagged Myo5 constructs purified from yeast were used instead of the GST construct purified from *E. coli*.

Fluorescence microscopy

Fluorescence micrographs in Figure 1 were obtained with an *Axiophot* fluorescence microscope (Zeiss) equipped with a GFP filter (excitation 470/40, LP520) and an Olympus DP70 camera. Cells were grown to mid-log phase, harvested, diluted in a small volume of SDC medium and visualized on poly-lysine-coated slides. Rhodamine-actin in the *in vitro* polymerization assay was observed using a rhodamine filter (excitation BP545/30, emission LP590). For the time-lapse fluorescence microscopy, yeast expressing GFP-Myo5 were grown to mid-log phase in SDC medium. Time-lapse videos were collected from cells immobilized in 0.8% low-melt agarose prepared in complete synthetic medium. A Perkin Elmer UltraView ERS Spinning-Disk microscope, equipped with Argon (488, 514 nm), Argon/Krypton (568 nm) and HeNe (405, 440, 640 nm) Lasers, a 405/488/568/640 Dichroic and a Hamamatsu C9100-50 EMCCD camera was used to collect images. A ×63 1.4NA Oil DIC Plan-Apochromat objective was used for all movies. Time-lapse microscopy images were taken every 2 s and were acquired/processed using Volocity from Improvision (Perkin Elmer). Volocity files were converted to multi-tiff for image processing and to csv for relative intensity fluorescence analysis using Microsoft Excel. Average, standard deviation and *P*-values for the Student's *t*-test were calculated with Microsoft Excel. All images were collected with identical sensitivity and exposure times of 600 ms, 500 ms and 1 s for GFP-Myo5, Abp1-RFP and Sla1-mCherry, respectively. Only bright, well-defined patches were considered for further analysis.

For analysis of arrival and departure times of GFP-Myo5 relative to Sla1-mCherry or Abp1-RFP, relative fluorescence intensity (RFI) curves plotted against time (s) were calculated for each pair and the time point when Sla1-mCherry or Abp1-RFP reached RFI = 0.5 was subtracted from the time point when GFP-Myo5 reached RFI = 0.5 either before (arrival) or after (departure) the time point when Sla1-mCherry or Abp1-RFP reached RFI = 1 (see Figures 5 and 7).

Supplementary data

Supplementary data are available at *The EMBO Journal* Online (http://www.embojournal.org).

Acknowledgements

We thank M Pons, J Pérez and M Cid for technical assistance. This work was supported by BUF2005-04089, BFU2008-03500 and CSD2009-00016 (MIG) and NIH R01 GM055796 (SKL) grants. HG was a recipient of a predoctoral fellowship from the Generalitat de Catalunya. F-ZI is a Ramon y Cajal postdoctoral fellow. JG and VR are supported by JAE postdoctoral and technician contracts from the CSIC, respectively. JRC was supported by a NIH training grant T32-HL07188 and an American Heart Association postdoctoral fellowship 6-6253Y.

Conflict of interest

The authors declare that they have no conflict of interest.

References

Adams RJ, Pollard TD (1989) Binding of myosin I to membrane lipids. *Nature* **340:** 565–568

Anderson BL, Boldogh I, Evangelista M, Boone C, Greene LA, Pon LA (1998) The Src homology domain 3 (SH3) of a yeast type I myosin, Myo5p, binds to verprolin and is required for targeting to sites of actin polarization. *J Cell Biol* **141:** 1357–1370

Audhya A, Loewith R, Parsons AB, Gao L, Tabuchi M, Zhou H, Boone C, Hall MN, Emr SD (2004) Genome-wide lethality screen identifies new PI4,5P2 effectors that regulate the actin cytoskeleton. *EMBO J* **23:** 3747–3757

Bose A, Guilherme A, Robida SI, Nicoloro SM, Zhou QL, Jiang ZY, Pomerleau DP, Czech MP (2002) Glucose transporter recycling in response to insulin is facilitated by myosin Myo1c. *Nature* **420:** 821–824

Brockerhoff SE, Davis TN (1992) Calmodulin concentrates at regions of cell growth in Saccharomyces cerevisiae. *J Cell Biol* **118:** 619–629

Cordonnier MN, Dauzonne D, Louvard D, Coudrier E (2001) Actin filaments and myosin I alpha cooperate with microtubules for the movement of lysosomes. *Mol Biol Cell* **12:** 4013–4029

Cyr JL, Dumont RA, Gillespie PG (2002) Myosin-1c interacts with hair-cell receptors through its calmodulin-binding IQ domains. *J Neurosci* **22:** 2487–2495

Doberstein SK, Baines IC, Wiegand G, Korn ED, Pollard TD (1993) Inhibition of contractile vacuole function *in vivo* by antibodies against myosin-I. *Nature* **365:** 841–843

Doberstein SK, Pollard TD (1992) Localization and specificity of the phospholipid and actin binding sites on the tail of Acanthamoeba myosin IC. *J Cell Biol* **117:** 1241–1249

Dower WJ, Miller JF, Ragsdale CW (1988) High efficiency transformation of E. coli by high voltage electroporation. *Nucleic Acids Res* **16:** 6127–6145

Dulic V, Egerton M, Elguindi I, Raths S, Singer B, Riezman H (1991) Yeast endocytosis assays. *Methods Enzymol* **194:** 697–710

Durrbach A, Collins K, Matsudaira P, Louvard D, Coudrier E (1996) Brush border myosin-I truncated in the motor domain impairs the distribution and the function of endocytic compartments in an hepatoma cell line. *Proc Natl Acad Sci USA* **93:** 7053–7058

Durrbach A, Raposo G, Tenza D, Louvard D, Coudrier E (2000) Truncated brush border myosin I affects membrane traffic in polarized epithelial cells. *Traffic* **1:** 411–424

Evangelista M, Klebl BM, Tong AH, Webb BA, Leeuw T, Leberer E, Whiteway M, Thomas DY, Boone C (2000) A role for myosin-I in actin assembly through interactions with Vrp1p, Bee1p, and the Arp2/3 complex. *J Cell Biol* **148:** 353–362

Fath KR, Trimbur GM, Burgess DR (1994) Molecular motors are differentially distributed on Golgi membranes from polarized epithelial cells. *J Cell Biol* **126:** 661–675

Galletta BJ, Chuang DY, Cooper JA (2008) Distinct roles for Arp2/3 regulators in actin assembly and endocytosis. *PLoS Biol* **6:** e1

Geiser JR, van Tuinen D, Brockerhoff SE, Neff MM, Davis TN (1991) Can calmodulin function without binding calcium? *Cell* **65:** 949–959

Geli MI, Lombardi R, Schmelzl B, Riezman H (2000) An intact SH3 domain is required for myosin I-induced actin polymerization. *EMBO J* **19:** 4281–4291

Geli MI, Riezman H (1996) Role of type I myosins in receptor-mediated endocytosis in yeast. *Science* **272:** 533–535

Geli MI, Riezman H (1998) Endocytic internalization in yeast and animal cells: similar and different. *J Cell Sci* **111** (Part 8)**:** 1031–1037

Geli MI, Wesp A, Riezman H (1998) Distinct functions of calmodulin are required for the uptake step of receptor-mediated endocytosis in yeast: the type I myosin Myo5p is one of the calmodulin targets. *EMBO J* **17:** 635–647

Harlow E, Lane D (1988) *Antibodies, a Laboratory Manual*. NY: Cold Spring Harbor Laboratory Press

Hayden SM, Wolenski JS, Mooseker MS (1990) Binding of brush border myosin I to phospholipid vesicles. *J Cell Biol* **111:** 443–451

Hirono M, Denis CS, Richardson GP, Gillespie PG (2004) Hair cells require phosphatidylinositol 4,5-bisphosphate for mechanical transduction and adaptation. *Neuron* **44:** 309–320

Huber LA, Fialka I, Paiha K, Hunziker W, Sacks DB, Bahler M, Way M, Gagescu R, Gruenberg J (2000) Both calmodulin and the unconventional myosin Myr4 regulate membrane trafficking along the recycling pathway of MDCK cells. *Traffic* **1:** 494–503

Hwang KJ, Mahmoodian F, Ferretti JA, Korn ED, Gruschus JM (2007) Intramolecular interaction in the tail of Acanthamoeba myosin IC between the SH3 domain and a putative pleckstrin homology domain. *Proc Natl Acad Sci USA* **104:** 784–789

Idrissi FZ, Grotsch H, Fernandez-Golbano IM, Presciatto-Baschong C, Riezman H, Geli MI (2008) Distinct acto/myosin-I structures associate with endocytic profiles at the plasma membrane. *J Cell Biol* **180:** 1219–1232

Idrissi FZ, Wolf BL, Geli MI (2002) Cofilin, but not profilin, is required for myosin-I-induced actin polymerization and the endocytic uptake in yeast. *Mol Biol Cell* **13:** 4074–4087

Ishikawa T, Cheng N, Liu X, Korn ED, Steven AC (2004) Subdomain organization of the Acanthamoeba myosin IC tail from cryo-electron microscopy. *Proc Natl Acad Sci USA* **101:** 12189–12194

Ito H, Fukuda Y, Murata K, Kimura A (1983) Transformation of intact yeast cells treated with alkali cations. *J Bacteriol* **153:** 163–168

Jonsdottir GA, Li R (2004) Dynamics of yeast Myosin I: evidence for a possible role in scission of endocytic vesicles. *Curr Biol* **14:** 1604–1609

Jontes JD, Ostap EM, Pollard TD, Milligan RA (1998) Three-dimensional structure of Acanthamoeba castellanii myosin-IB (MIB) determined by cryoelectron microscopy of decorated actin filaments. *J Cell Biol* **141:** 155–162

Jung G, Hammer III JA (1990) Generation and characterization of Dictyostelium cells deficient in a myosin I heavy chain isoform. *J Cell Biol* **110:** 1955–1964

Jung G, Remmert K, Wu X, Volosky JM, Hammer III JA (2001) The Dictyostelium CARMIL protein links capping protein and the Arp2/3 complex to type I myosins through their SH3 domains. *J Cell Biol* **153:** 1479–1497

Krendel M, Osterweil EK, Mooseker MS (2007) Myosin 1E interacts with synaptojanin-1 and dynamin and is involved in endocytosis. *FEBS Lett* **581:** 644–650

Kubler E, Schimmoller F, Riezman H (1994) Calcium-independent calmodulin requirement for endocytosis in yeast. *EMBO J* **13:** 5539–5546

Kuriyan J, Cowburn D (1997) Modular peptide recognition domains in eukaryotic signaling. *Annu Rev Biophys Biomol Struct* **26:** 259–288

Laemmli UK (1970) Cleavage of structural proteins during the assembly of the head of bacteriophage T4. *Nature* **227:** 680–685

Lechler T, Jonsdottir GA, Klee SK, Pellman D, Li R (2001) A two-tiered mechanism by which Cdc42 controls the localization and activation of an Arp2/3-activating motor complex in yeast. *J Cell Biol* **155:** 261–270

Lechler T, Shevchenko A, Li R (2000) Direct involvement of yeast type I myosins in Cdc42-dependent actin polymerization. *J Cell Biol* **148:** 363–373

Lee WL, Bezanilla M, Pollard TD (2000) Fission yeast myosin-I, Myo1p, stimulates actin assembly by Arp2/3 complex and shares functions with WASp. *J Cell Biol* **151:** 789–800

Lee WL, Ostap EM, Zot HG, Pollard TD (1999) Organization and ligand binding properties of the tail of Acanthamoeba myosin-IA. Identification of an actin-binding site in the basic (tail homology-1) domain. *J Biol Chem* **274:** 35159–35171

Lieto-Trivedi A, Coluccio LM (2008) Calcium, nucleotide, and actin affect the interaction of mammalian Myo1c with its light chain calmodulin. *Biochemistry* **47:** 10218–10226

Miyata H, Bowers B, Korn ED (1989) Plasma membrane association of Acanthamoeba myosin I. *J Cell Biol* **109:** 1519–1528

Muniz M, Morsomme P, Riezman H (2001) Protein sorting upon exit from the endoplasmic reticulum. *Cell* **104:** 313–320

Neuhaus EM, Soldati T (2000) A myosin I is involved in membrane recycling from early endosomes. *J Cell Biol* **150:** 1013–1026

Novak KD, Peterson MD, Reedy MC, Titus MA (1995) Dictyostelium myosin I double mutants exhibit conditional defects in pinocytosis. *J Cell Biol* **131:** 1205–1221

Novak KD, Titus MA (1997) Myosin I overexpression impairs cell migration. *J Cell Biol* **136:** 633–647

Oberholzer U, Iouk TL, Thomas DY, Whiteway M (2004) Functional characterization of myosin I tail regions in Candida albicans. *Eukaryotic cell* **3:** 1272–1286

Ohya Y, Botstein D (1994) Structure-based systematic isolation of conditional-lethal mutations in the single yeast calmodulin gene. *Genetics* **138:** 1041–1054

Phillips KR, Tong S, Goodyear R, Richardson GP, Cyr JL (2006) Stereociliary myosin-1c receptors are sensitive to calcium chelation and absent from cadherin 23 mutant mice. *J Neurosci* **26:** 10777–10788

Pollard TD, Doberstein SK, Zot HG (1991) Myosin-I. *Annu Rev Physiol* **53:** 653–681

Raposo G, Cordonnier MN, Tenza D, Menichi B, Durrbach A, Louvard D, Coudrier E (1999) Association of myosin I alpha with endosomes and lysosomes in mammalian cells. *Mol Biol Cell* **10:** 1477–1494

Rohatgi R, Ho HY, Kirschner MW (2000) Mechanism of N-WASP activation by CDC42 and phosphatidylinositol 4, 5-bisphosphate. *J Cell Biol* **150:** 1299–1310

Sambrook J, Fritsch EF, Maniatis T (1989) *Molecular Cloning: A Laboratory Manual*, 2nd ed. Cold Spring Harbor Laboratory Press

Serrano R (1988) H+-ATPase from plasma membranes of Saccharomyces cerevisiae and Avena sativa roots: purification and reconstitution. *Methods Enzymol* **157:** 533–544

Seth A, Otomo C, Rosen MK (2006) Autoinhibition regulates cellular localization and actin assembly activity of the diaphanous-related formins FRLalpha and mDia1. *J Cell Biol* **174:** 701–713

Sherman S, Fink G, Lawrence C (1974) *Methods in Yeast Genetics*. Cols Spring Harbor, NY: Cold Spring Harbor Laboratory Press

Sun Y, Carroll S, Kaksonen M, Toshima JY, Drubin DG (2007) PtdIns(4,5)P2 turnover is required for multiple stages during clathrin- and actin-dependent endocytic internalization. *J Cell Biol* **177:** 355–367

Sun Y, Martin AC, Drubin DG (2006) Endocytic internalization in budding yeast requires coordinated actin nucleation and myosin motor activity. *Dev Cell* **11:** 33–46

Swanljung-Collins H, Collins JH (1992) Phosphorylation of brush border myosin I by protein kinase C is regulated by Ca(2+)-stimulated binding of myosin I to phosphatidylserine concerted with calmodulin dissociation. *J Biol Chem* **267:** 3445–3454

Tang N, Lin T, Ostap EM (2002) Dynamics of myo1c (myosin-ibeta) lipid binding and dissociation. *J Biol Chem* **277:** 42763–42768

Temesvari LA, Bush JM, Peterson MD, Novak KD, Titus MA, Cardelli JA (1996) Examination of the endosomal and lysosomal pathways in Dictyostelium discoideum myosin I mutants. *J Cell Sci* **109**(Part 3)**:** 663–673

Terrak M, Rebowski G, Lu RC, Grabarek Z, Dominguez R (2005) Structure of the light chain-binding domain of myosin V. *Proc Natl Acad Sci USA* **102:** 12718–12723

Titus MA, Wessels D, Spudich JA, Soll D (1993) The unconventional myosin encoded by the myoA gene plays a role in Dictyostelium motility. *Mol Biol Cell* **4:** 233–246

Tong AH, Drees B, Nardelli G, Bader GD, Brannetti B, Castagnoli L, Evangelista M, Ferracuti S, Nelson B, Paoluzi S, Quondam M, Zucconi A, Hogue CW, Fields S, Boone C, Cesareni G (2002) A combined experimental and computational strategy to define protein interaction networks for peptide recognition modules. *Science* **295:** 321–324

van Tuinen E, Riezman H (1987) Immunolocalization of glyceraldehyde-3-phosphate dehydrogenase, hexokinase, and carboxypeptidase Y in yeast cells at the ultrastructural level. *J Histochem Cytochem* **35:** 327–333

Wessels D, Murray J, Jung G, Hammer III JA, Soll DR (1991) Myosin IB null mutants of Dictyostelium exhibit abnormalities in motility. *Cell Motil Cytoskeleton* **20:** 301–315

Whittaker M, Milligan RA (1997) Conformational changes due to calcium-induced calmodulin dissociation in brush border myosin I-decorated F-actin revealed by cryoelectron microscopy and image analysis. *J Mol Biol* **269:** 548–557

Wu XS, McNeil BD, Xu J, Fan J, Xue L, Melicoff E, Adachi R, Bai L, Wu LG (2009) Ca(2+) and calmodulin initiate all forms of endocytosis during depolarization at a nerve terminal. *Nature Neurosci* **12:** 1003–1010

Yamashita RA, Osherov N, May GS (2000) Localization of wild type and mutant class I myosin proteins in Aspergillus nidulans using GFP-fusion proteins. *Cell Motil Cytoskeleton* **45:** 163–172

